Conserved cysteine residues in Kaposi's sarcoma herpesvirus ORF34 are necessary for viral production and viral pre-initiation complex formation.

Tadashi Watanabe[1,*], Akshara Narahari[2], Esha Bhardwaj[2], Kazushi Kuriyama[1], Mayu Nishimura[3], Taisuke Izumi[2], Masahiro Fujimuro[3], and Shinji Ohno[1,*]

1: Department of Virology, Graduate School of Medicine, University of the Ryukyus, 207 Uehara, Nishihara, Nakagami, Okinawa, 903-0215, Japan

2: Department of Biology, Saint Joseph's University, Philadelphia, PA 19104, U.S.A.

3: Department of Cell Biology, Kyoto Pharmaceutical University, 1 Misasagi-Shichono, Yamashina, Kyoto 607-8412, Japan.

*: Address correspondence to Tadashi Watanabe, Ph.D. and Shinji Ohno, M.D., Ph.D., Department of Virology, Graduate School of Medicine, University of the Ryukyus, 207 Uehara, Nishihara, Nakagami, Okinawa, 903-0215, Japan; Tel: +81-98-895-1131 and +81-98-895-1708

E-mail: T.W.; twatanab@med.u-ryukyu.ac.jp, S.O.; soono@med.u-ryukyu.ac.jp

Running title: Profiling of the conserved residues in KSHV ORF34

ABSTRACT

Kaposi's sarcoma herpesvirus (KSHV) ORF34 is a component of the viral pre-initiation complex (vPIC), a highly conserved piece of machinery essential for late gene expression among beta- and gamma-herpes viruses. KSHV ORF34 is also estimated to be a hub protein, associated with the majority of vPIC components. However, the precise mechanisms underlying how the ORF34 molecule contributes to the vPIC function, including the binding manner to other vPIC components, remain unclear. Therefore, we constructed ORF34 alanine-scanning mutants, in which amino-acid residues that were conserved among other herpesviruses had been replaced by alanine. The mutants were analyzed for their binding functions to other vPIC factors, and then were evaluated for their recovering ability of viral production using the cells harboring ORF34-deficient KSHV-BAC. The results demonstrated that at least four cysteines conserved in ORF34 were crucial for binding to other vPIC components, ORF24 and ORF66, virus production, and late gene transcription and expression. Based on the amino acid sequence of ORF34, these four cysteines were expected to constitute a pair of C-X_n-C consensus motifs. An artificial intelligence-predicted structure model revealed that the four cysteines were present tetrahedrally in an intramolecular fashion. Another prediction algorithm indicated the possible capture of metal cations by ORF34. Furthermore, it was experimentally observed that the elimination of cations by a selective chelator resulted in the loss of ORF34's binding ability to other vPIC components. In conclusion, our results suggest the functional importance of KSHV ORF34 conserved cysteines for vPIC components assembly and viral replication.

IMPORTANCE

The gamma- and beta-herpesvirus family conserve the viral-factor based mechanism for initiating viral late gene transcription. This viral pre-initiation complex (vPIC) is a functional analog to cellular PIC consisting of general transcriptional factors. We focused on KSHV ORF34, an essential factor for viral replication as a vPIC component. The precise mechanism underlying vPIC formation and critical domain structure of ORF34 for its function are presently unclear. Therefore, we investigated the contribution of conserved amino-acid residues among ORF34 homologs to virus production, late gene expression, and interaction with other vPIC components. We demonstrated for the first time that four conserved cysteines (C170, C175, C256, and C259) in ORF34 are essential for vPIC formation, late gene transcription, and viral production. Importantly, the predicted structure model and biochemical experiment provide evidence showing that these four conserved cysteines are present in a tetrahedral formation which helped to maintain metal cation.

Introduction

Kaposi's sarcoma herpesvirus (KSHV), a human herpesvirus, causes several malignancies associated with epithelial cells and B-lymphocytes (1). The representative epithelial cancer caused by KSHV is Kaposi's sarcoma (KS), and representative B-lymphocyte cancers are multicentric Castleman's disease (MCD) and primary effusion lymphoma (PEL) (2-5). In addition, KSHV also causes an inflammatory disorder known as KSHV inflammatory cytokine syndrome (KICS) (1, 2, 5). Elevated levels of cytokines, such as IL-6 and IL-10, are also found in KICS patients.

KSHV, also known as human gammaherpesvirus-8 (HuGHV8) or human herpesvirus-8 (HHV-8), is classified into the subfamily *Gammaherpesvirinae*, which also includes Epstein-Barr virus (EBV) (6-8). Other human herpesviruses are classified into the subfamilies *Alphaherpesvirinae* (HSV-1, HSV-2, and VZV) and *Betaherpesvirinae* (CMV, HHV-6A, HHV-6B, HHV-7) (7, 8). These classifications are partly based on biological properties and epidemiological features. Among human herpesviruses, *Alphaherpesvirinae* and *Betaherpesvirinae* are not directly linked to oncogenicity; only *Gammaherpesvirinae*, *i.e.* KSHV and EBV, have direct pathogenicity for developing malignant neoplasms (3, 6, 9).

The viral gene expression is essential for viral genome replication and producing progeny. After the viral entry, herpesviruses initially express genes, called latent genes, thereby establishing and maintaining latency and then epigenetically silencing other viral genes (10). In KSHV, transitioning from latency to the virus production phase, known as lytic infection, requires viral reactivation. Such reactivation can be caused by various stimuli, environmental changes in the infected cells, and cellular signaling alterations. Reactivation results in upregulating the expression of KSHV-coding genes, called lytic genes (11-13). The lytic gene expression processes of KSHV are roughly classified into three sequential steps, according to

the KSHV life cycle progression: immediate-early (IE) genes, early (E) genes, and late (L) genes (1, 14, 15).

The lytic phase is triggered by the viral transcription factor ORF50/k-RTA, an IE gene enabling the shift from latency to producing mode by the activation of lytic gene promoters (16, 17). E-genes related to viral DNA genome replication are then transcribed. Finally, L-genes, including viral structure proteins, capsid, and envelope proteins, are expressed. Such serial expression enables KSHV to efficiently produce virus particles without the stagnation of diverse KSHV-coding gene products, including proteins and functional RNAs (lncRNA and/or miRNA), in the host sequential mechanisms of transcription and translation (1, 18).

Gamma- and beta-herpesviruses, but not alpha-herpesviruses, have an additional characteristic system for regulating L-gene expression called the viral pre-initiation complex (vPIC), composed of several viral proteins coded by lytic genes (19). Most viruses employ the host transcription machinery, including the preinitiation complex (PIC), consisting of TATA-binding protein (TBP) binding to the TATA-box sequences and other general transcription factors (GTFs). Gamma- and beta-herpesviruses also utilize the host cellular PIC machinery for IE- and E-gene expression; however, some L-genes from these two herpesvirus families start their transcription with vPIC (19). Six KSHV proteins (ORF18, ORF24, ORF30, ORF31, ORF34, and ORF66) are essential for viral replication and have been shown to be components of vPIC (20-26). KSHV ORF24 is thought to be a functional analog of TBP that directly binds to a TATA-box-like sequence, the TATT-motif, present at the transcription start site (TSS) of some L-genes. ORF24 also contributes to directly recruiting the RNA polymerase II (RNAPII) complex to L-gene TSS and to initiating mRNA transcription (21, 27). Other vPIC components, namely ORF18, ORF30, ORF31, and ORF66, are suggested to be involved in the generation of the protein-protein interaction network with ORF24 via ORF34. ORF34 serves as a network hub for gathering ORF18, ORF31, and ORF66 to ORF24 (20-26). ORF30 binds to only ORF18,

not to other vPIC components (21, 26, 28). This protein complex composed of each component is also indispensable for viral L-gene transcription (20-26). However, the precise interaction mechanisms and other functions involved in transcription initiation, including single components and entire complexes, are poorly understood.

Our previous work on KSHV vPIC revealed the necessity of KSHV ORF34 for viral replication as a vPIC component (20). The middle regions of ORF34 are essential for binding to ORF18, ORF31, and ORF66. It was demonstrated that the C-terminal region of ORF34 was also required for binding to ORF24 and virus production. These results indicated that the ORF34 C-terminal is responsible for vPIC formation by anchoring other components to the viral TBP ORF24. However, other molecular information on ORF34, including its domain structure and related functions, is unclear.

We therefore investigated the importance of conserved amino-acid residues on KSHV ORF34. A total of 18 alanine-substituted mutants of KSHV ORF34 were evaluated for their role in virus replication and vPIC formation. These results combined with those from an artificial intelligence (AI)-predicted structure model have highlighted new perspectives concerning the relationship between the ORF34 function and its structure.

Results

Conserved amino-acid residues between KSHV ORF34 and beta- and gamma-herpes viral homologs

One of the issues tackled in the present study is unveiling the important regions of ORF34 in the functional expression of the vPIC, including more precise details than in our previous research (20). As described previously, the vPIC machinery and its viral components are broadly conserved between the beta- and gamma-herpesvirus families (19). It is strongly believed that the important domains or structures in each protein functioning, such as vPIC components, would be conserved among viral homologs. In general, conserved domains and structures often consist of conserved amino-acid residues. Thus, to clarify the conserved amino-acid residues, the amino-acid sequence alignments of the KSHV ORF34 and other herpes virus homologs are depicted and marked with a gray background (Fig. 1).

The alignment data showed that 7 amino-acid residues at the N-terminal of KSHV ORF34 and 21 at the C-terminal were conserved among beta- and gamma-herpesviruses. As these conserved residues of ORF34 were predicted to be functionally important regions within ORF34, we generated ORF34 mutants in which these residues were substituted by alanine. After excluding the conserved prolines, the mutation of which would disrupt the local and whole protein backbone, we prepared 18 expression plasmids with single- or double-alanine substitutions at the conserved amino-acid residues to generate ORF34 alanine-scanning mutants. These 18 mutants are also depicted in Figure 1.

Physical interactions between ORF34 alanine-scanning mutants and vPIC components

KSHV ORF34 is reported to directly interact with the majority of vPIC components (ORF18, ORF24, ORF31, and ORF66), except for ORF30 (20, 21). Based on these findings, KSHV ORF34 has been thought to be a hub protein forming vPIC. To analyze the contribution of

ORF34 conserved residues to the interaction with other vPIC components, bindings between ORF34 alanine-scanning mutants and the other components were assessed through pull-down experiments (Figs. 2 and 3).

The N-terminal region (1-400 a.a.) of ORF24 (ORF24 binding domain; ORF24 BD) binds to ORF34, and R328 on ORF24 is essential for ORF34 binding (21). To facilitate ORF24 detection, we prepared expression plasmids of the ORF24 BD (6xMyc-tagged ORF24 BD [1-400 a.a.]). 293T cells were co-transfected with 2xS-tagged ORF34 alanine-scanning mutants and 6xMyc-ORF24 BD, 3xFLAG-ORF66, 3xFLAG-ORF18, and 3xFLAG-ORF31 as indicated in each figure. The cell extracts were then subjected to pull-down experiments. Initially, we profiled the interaction ability of ORF34 mutants to ORF24 BD and ORF66. As a result, our ORF34 mutants exhibited various features in association with another vPIC component. Notably, ORF34 C170A, C175A, C256A, and C259A remarkably decreased or lost their binding ability to both ORF24 and ORF66 (Fig. 2b-c and 2e-f). In addition, G165A, L188A/L189A, Y194A, and Q264A/N265A also lost their interaction with ORF66 (Fig. 2d-f). Conversely, no defects in the interaction ability for ORF18 and ORF31 were observed in any ORF34 alanine-scanning mutants (Fig. 3). Our previous study using ORF34 deletion mutants showed that the 100-150 a.a. region of ORF34 was responsible for binding to ORF18 and ORF31 (20). However, the ORF34 alanine-scanning mutants in the present study did not include any alanine-substituted residues from that region. Therefore, the binding data of the ORF34 alanine-scanning mutants in the present study gave concordant results.

Characterization of ORF34 conserved residues concerning KSHV production

The transcriptional initiation through the vPIC is essential for KSHV production. To evaluate the functional importance of ORF34 conserved residues in vPIC, we considered an analysis of progeny virus production to be the most appropriate method. Therefore, a complementation assay using ORF34-deficient virus-producing cells stably expressing ORF34 alanine-scanning mutants was conducted.

First, we established iSLK cell lines harboring KSHV ΔORF34-BAC (iSLK-Δ34) and iSLK cell lines harboring KSHV ΔORF34 Revertant-BAC (iSLK-Δ34Rev). Those BACmids were constructed in our previous study (20). 3xFLAG-tagged ORF34 WT was then transfected into the iSLK-Δ34 cells. As the control, a control plasmid was transfected into iSLK-Δ34 and iSLK-Δ34Rev cells. To generate stable cell lines, these transfected cells were subjected to drug selection. The complemented exogenous ORF34 in iSLK-Δ34 cells was confirmed (Fig. 4a). Using these cell lines, we evaluated the recovery ability of exogenous ORF34 in iSLK-Δ34 cells (Fig. 4b). The cell lines were cultured with conditioned medium containing sodium butyrate (NaB; an HDAC inhibitor that accelerates gene expression) and doxycycline (Dox; an activator for Tet-on system. Using this system equipped in an iSLK cell, Dox induces ORF50/k-RTA and thereby triggering the lytic phase) for three days. The encapsidated KSHV genome was purified from the cultured supernatant and quantified by quantitative polymerase chain reaction (qPCR).

The results showed that ORF34 deficiency causes a notable decrease in virus production, and exogenous ORF34 in deficient cells complements most of the virus production. These results also underscore the need for ORF34 for KSHV viral production.

The same strategy was employed for the evaluation of the 18 conserved amino-acid mutants of ORF34. Each FLAG-tagged ORF34 mutant expression plasmid was transfected into iSLK-Δ34 cells and selected for the generation of stable cell lines, as indicated, and the protein

expression was confirmed (lower panels in Fig. 4c-e). The KSHV production in these cell lines was then compared with that in the iSLK-Δ34/ORF34 WT cells (upper graphs in Fig. 4c-e). The results showed that the complementation of ORF34 G165A, S168A, and G182A rescued the virus production in iSLK-Δ34 cells, indicating that these substituted residues do not contribute to the ORF34 role in virus release. In contrast, ORF34 E41A/T42A-, F47A-, D154A-, C170A-, C175A-, L188A/L189A-, C256A-, C259A-, Q264A/N265A-, and Y310A-expressing cell lines did not show a recovered virus production, indicating that these mutated residues do contribute to the ORF34 wild-type role in virus release. Exogenous ORF34 V50A, W160A, Y194A, Y215A, and R234A showed partial complementation to the loss of ORF34 in iSLK-Δ34 cells.

Role of ORF34 conserved residues in viral gene transcription and protein expression

The main function of vPIC in the KSHV life cycle is the initiation of L-gene expression. To determine whether or not the virus production recovery abilities among ORF34 WT and mutants were due to KSHV L-gene expression, we analyzed the expression of the representative genes in each step (*i.e.,* K4 as IE, ORF6 as E, and K8.1 as L-gene) based on the mRNA (Fig. 5a-c) and protein expression (Fig. 5d-f). The stable cell lines, iSLK-Δ34 cells complemented with ORF34 WT or alanine-scanning mutants, were stimulated with NaB and Dox for three days. Total RNA was extracted from each cell line and then was subjected to reverse transcription qPCR (RT-qPCR).

The results showed that the transcription of K8.1 in iSLK-Δ34 cells expressing ORF34 E41A/T42A, F47A, D154A, C170A, C175A, L188A/L189A, Y194A, C256A, C259A, Q264A/N265A, and Y310A was markedly reduced compared with that in iSLK-Δ34/WT cells but differed little from that in iSLK-Δ34/Control cells. In contrast, the transcription of K8.1 was complemented by G165A, S168A, G182A, and Y215A (Fig. 5a-c). The transcription levels

of K4 and ORF6 were almost equal among all iSLK-Δ34 cell lines expressing ORF34 WT or its mutants. In parallel with the above RNA sampling, we prepared protein samples from each complemented iSLK-Δ34 cell line. The protein expression of the representative E gene K-bZIP in each cell line showed no marked differences among cell lines (Fig. 5d-f; upper middle panels). In contrast, we observed notable differences in the K8.1 protein expression among cell lines. The K8.1 protein expression was rescued in ORF34 G165A-, S168A-, and Y215A-expressing iSLK-Δ34 cell lines and was partially complemented in ORF34 R234A- and G182A-expressing cells. The protein expression of K8.1 was unable to be rescued in other mutants (Fig. 5d-f; upper panels). These differences in the K8.1 protein expression among cell lines were in good agreement with the data on K8.1 mRNA obtained by qPCR.

Profiling of ORF34 alanine-scanning mutants on vPIC-related parameters

The data obtained in this study (Fig. 2, 4-5) are summarized and visualized by a heatmap with a dendrogram of hierarchical clustering (Fig. 6). The extracted parameters were i) binding to ORF66 (Fig. 2d-f), ii) binding to ORF24BD (Fig. 2a-e), iii) K8.1 mRNA expression (Fig. 5a-e), iv) K8.1A/B protein expression (Fig. 5d-f), and v) KSHV production (Fig. 4c-e). Binding to ORF18 and ORF31 (Fig. 3) were excluded because no differences between ORF34 WT and its mutant were observed. ORF34 mutants were roughly classified into four groups according to the visualized dendrogram (Fig. 6).

- Group 1: The mutants were able to complement virus production in iSLK-Δ34 cells. These substituted amino-acid residues are thus not essential for the entire vPIC function.
- Group 2: The mutants failed to complement virus production and showed a decreased binding ability to both ORF24 and ORF66. The conserved residues on the mutants were inferred to be essential for the vPIC function via complex formation.
- Group 3: While the mutants did not rescue virus production, the binding ability to

ORF24 and ORF66 was unaltered. These mutation sites are thus important for the vPIC machinery. The mechanism underlying the contribution of these residues to the vPIC function might not be direct interaction with ORF24 and ORF66. However, the precise details are unknown.

- Group 4: The mutants maintained their binding to ORF24 (but not to ORF66) and tended to fail to complement virus production. These mutated sites might be related to the vPIC function via ORF66 binding.

One of the notable results was that the ORF34 S168A mutant showed over-complementation in virus production, 10 times more than ORF34 WT. Thus, the S168A mutant was out of the range of other mutants in the dendrogram. Almost equal to ORF34 WT, ORF34 S168A held the binding ability to ORF24 and ORF66. Therefore, further studies on S168A would be necessary to clarify the mechanism of vPIC regulation. Both G165A and Y215A reduced interaction with ORF66 and maintained or mildly reduced its viral production, respectively. These sites therefore likely contributed to the direct association between the two viral proteins of ORF34 and ORF66. However, considering the small influence on the virus production and L-gene expression in each KSHV-producing cell line, other factors brought about by a virus infection, including vPIC components, might help restore the association between ORF34 G165A/Y215A and ORF66.

At a minimum, our obtained data (Fig. 2, 4-5) and grouping of ORF34 mutants by hierarchical clustering (Fig. 6) demonstrated that ORF34 C170A, C175A, C256A, and C259A, which were categorized into Group 1, lost most of their interaction with ORF24 and ORF66 and the virus production recovery ability. This suggests that these conserved cysteines are crucial for the ORF34 function in KSHV replication. In addition, on reframing these residues in an amino-acid sequence (Fig. 1), C170-R171-A172-D173-C174-C175 and C256-L257-L258-C259 form the consensus motif sequences C-X_4-C and C-X_2-C, respectively. These two

consensus sequences (C-X_n-C) are well known to form ion-capturing domains, such as the zinc finger domain.

AI-predicted structure model of KSHV ORF34 and conserved cysteines

Prediction structure models by the deep-learning algorithm have been widely used as powerful tools for life-science fields, including virology. We previously applied that to a partial vPIC protein-protein interaction model (28). The structure of KSHV ORF34 is predicted by Alphafold2, an algorithm for predicting the protein structure from the amino-acid sequence (29). The entire predicted structure was visualized by an illustration model labeled with pLDDT, which is the prediction confidence score (Fig. 7a; left panel). Rotated structures were also visualized (Fig. 8a). The four conserved cysteines (C170, C175, C256, and C259A) and their sidechains are highlighted with green in the enclosed area (Fig. 7a; middle panel). Interestingly, the pair of consensus C-X_n-C motifs consisting of the conserved cysteines were nearly symmetric within ORF34. Side chains of cysteines were re-labeled with the constituent sulfur atom (Fig. 7a; right panel). Other conserved amino-acid residues of ORF34 in the model are highlighted with magenta (Fig. 8b and 8c). The two-dimensional (2D) plot of the pLDDT score versus amino-acid residues, which emphasizes the conserved amino-acid residues of the alanine-mutation target, showed that the local structure around the conserved amino acids had been predicted with high reliability (Fig. 7b). The predicted aligned error (PAE) plot indicates the predicted length of the alpha-carbon between each amino-acid in the model (Fig. 7c). The PAE plot provides information on domain prediction. Each green pixel indicates the predicted distance error between alpha-carbons of every amino-acid pair. Therefore, the green signal area indicates the clustering of amino-acid residues that may form a domain.

In our KSHV ORF34 predicted model, the PAE plot suggested the presence of a small domain in the N-terminal (approximately 1-50 a.a.) and a large domain structure in the C-

terminal (approximately 110-327 a.a.) (Fig. 7c). The plot also suggested that the disordered region (approximately 50-110 a.a.) connected the N- and C-terminal-predicted domains of ORF34. A disordered region of a protein is generally known to possesses no stable tertiary structure and provide flexibility linkage between domains with fixed structures.

Metal cation capturing by ORF34 and vPIC interactions

The existence of two pairs of consensus sequences (C-X_n-C) comprising four conserved cysteines and their symmetrical location on the predicted model strongly suggest the possibility of capturing divalent ions. To predict the ion-binding affinity due to the conserved cysteine residues on our simulated ORF34 structural model, we utilized the Metal Ion-Binding site prediction and modeling server (30) to estimate the potential binding ions and generate the docking model. The docking simulation predicted the binding residues of ORF34 with 16 metals and a total of 18 ions. The metal ions trapped by the residues of at least 1 of the consensus sequence cysteines (C170-C175 and/or C256-C259) and whose prediction scores were >3.0 are shown (Fig. 9a). Seven out of 18 ions (Zn^{2+}, Fe^{2+}, Fe^{3+}, Cd^{2+}, Hg^{2+}, Cu^{+}, and Pb^{2+}) were predicted to be captured by at least 1 of the C-X_n-C motifs of ORF34. Three metal ions (Zn^{2+}, Fe^{2+}, and Fe^{3+}) were highly anticipated to be captured by all four conserved cysteine residues (Fig. 9a), and Zn^{2+} (zinc) ion interaction was determined to be the dominant metal ion incorporated into ORF34 protein complexes according to the binding score. Based on these predictions, the structure model of ORF34 holding Zn^{2+} via four conserved cysteines is depicted in Figure 9b, as a representative model.

Next, we attempted to confirm that metal ion-capturing is crucial for the ORF34 function as the hub protein in vPIC. The *in vitro* binding ability of ORF34 to ORF24 or ORF66 was analyzed in the presence of the chelating agent TPEN, which has a higher affinity for heavy metal ions, including Zn, Fe, and Mn, than for Ca and Mg. The stability constant, a chemical

indicator of the chelating ability, of TPEN is highest for Zn among those five metal ions. Our results showed that TPEN interferes with the ORF34 association not only with the ORF24 BD (Fig. 9c) but also with ORF66 (Fig. 9d) in a concentration-dependent manner. These results suggest that capturing the heavy metal cation via conserved cysteines contained in the C-X_n-C consensus motif is important for the binding of ORF34 to other vPIC components (ORF24 and ORF66).

Discussion

In this study, we constructed alanine-substituted mutants of KSHV ORF34 with conserved amino-acid residues and broadly assessed their roles in viral replication and vPIC formation. After obtaining diverse information from our results, it was noteworthy that the four conserved cysteines (C170, C175, C256, and C259) in KSHV ORF34 were essential for the vPIC machinery. The mutants KSHV ORF34 C170A, C175A, C256A, and C259A were deficient in the association with ORF24 and ORF66 (Fig. 2 and 6). Furthermore, these mutants failed to complement virus production (Fig. 4 and 6) and the K8.1 gene transcription/protein expression (Fig. 5 and 6). These conserved cysteines of ORF34 might have some physical or virological significance in the protein structure and its functions. One of the findings supporting this speculation is the fact that the four cysteines comprised two pair of C-X_n-C consensus sequences (C170 and C175, and C256 and C259) (Fig. 1). The other is the AI-structure model predicted that the conserved cysteines are present in the inner side of ORF34 (Fig. 8c) and are placed in a roughly tetrahedral formation (Fig. 7a). Using the AlphaFold2 prediction model as our query, another prediction method (Metal Ion-Binding site prediction and modeling server; MIB2) provided data supporting the high probability of ion holding by the ORF34 conserved cysteines. This prediction demonstrated that the top candidate of metal cation captured by the double pair of conserved cysteines of ORF34 was zinc (Fig. 9a).

Further supporting the speculation concerning the physical or virological significance of the conserved cysteines, the binding ability of ORF34 to ORF24 and ORF66 was decreased in the presence of TPEN, a heavy metal cation chelator (Fig. 9c and 9d). Since TPEN has a higher affinity for zinc cation than for iron, it can exclude captured zinc more efficiently than it can iron and other metal cations. An article regarding the mathematical prediction for ion-binding site of metalloprotein revealed that AlphaFold2 was a useful and extensive tool for protein annotation for zinc ion binding (31). This report endorses our analysis strategy for

annotating the four conserved cysteines of ORF34 as the binding site of metal cation. Despite a lack of direct evidence, our prediction models and data from chelator treatment suggest that zinc was captured by ORF34 conserved cysteines. Concrete evidence concerning the protein structure, including the ion positions as determined by X-ray crystallography, nuclear magnetic resonance (NMR), or Cryogenic Electron Microscopy (Cryo-EM), is indispensable for confirming these findings.

For the host proteins composing cellular PIC, the functional analog of vPIC, capturing the ions is also important. Cellular PIC consists of TBP, GTFs, and multiple subunits of the RNAPII complex. Holding zinc via C-X_n-C motifs has been reported in several factors of cellular PIC, TFIIEα (32), TFIIB (33), TFIIS (34), and RPB9 (RNAPII subunit 9) (35). In TFIIEα, the loss of capturing ions from its structure induced a structural disturbance that negatively influenced its binding ability to other factors and transcription capability (32, 36). Zinc binding to TFIIB affects the structural rigidity and protein surface charge around the zinc-binding domain (37). Furthermore, the C-X_n-C motif is also indispensable for other vPIC components. We and Didychuck *et al.* demonstrated the importance of the C-X_n-C sequence of ORF66 for viral replication via vPIC formation (23, 24). In summary, the present findings and previous reports of host cellular PIC factors strongly support the notion that ion capturing via the C-X_n-C motif on KSHV ORF34 protein is crucial for maintaining the structural character and binding ability of ORF34 to other vPIC components, resulting in virus production via L-gene expression using vPIC machinery.

Our functional profiling of ORF34 conserved residues provided other valuable findings as well. KSHV ORF34 E41/T42, F47, and V50, which were classified into Group 3 (Fig. 6) and were present in the ORF34 N-terminal, are also essential residues for viral replication via L-gene expression while not affecting associations with other vPIC components. A simple speculation concerning the roles these residues play is that they are associated with unknown

host factors. The predicted algorithm AlphaFold2 suggested that ORF34 has an N-terminal domain and C-terminal domain. Those domains would be separated by the disorder region (Fig. 7 and 8). E41/T42, F47, and V50 exist in the N-terminal domain (Fig. 7 and 8). The other conserved amino-acid residues, including the responsible residues for the binding to other vPIC components, ORF24 and ORF66, exist in the C-terminal domain (Fig. 2, 6, 7a-c, 8). Other prediction algorithms for the disordered region, PrDOS (38) and DISOPRED3 (39), also suggest the presence of disordered regions of KSHV ORF34 at 64-70/89-108 a.a. and 92-107 a.a., respectively. Homology search results using the PDB database with AlphaFold2 demonstrated similarity between the N-terminal domain and some regulatory factor of the RNAPII complex.

Another hypothesis concerning the N-terminal conserved residues is based on EBV studies. It was reported that the phosphorylated T42 residue of BGLF3 (KSHV ORF34 homolog) was essential for the vPIC function and that phospho-T42 of BGLF3 was important for sub-complex formation among BFRF2 (KSHV ORF66 homolog) and BVLF1 (KSHV ORF18 homolog) (40). These reports demonstrated that two molecular interactions—BGLF3 binding to BFRF2 or BVLF1—were not affected by the phosphorylation state of T42, but three molecular interactions—the presence of BGLF3, BFRF2, and BVLF1—were positively dependent on phospho-T42 (40). Our alanine mutant, ORF34 E41A/T42A holds the mutation on analogous residues of EBV BGLF3 T42. Our observations of the ORF34 E41A/T42A mutant, including the interaction analysis, gene expression, and virus production, were well matched with a previous EBV study (40). Unfortunately, whether or not the subcomplex (*i.e.,* a protein subset of a larger functional protein complex) is present in KSHV has not yet been confirmed. Phospho-T42 in KSHV ORF34 may contribute to subcomplex formation, and the residues surrounding T42 (E41, F47, V50) may also work in coordination. Further research on this point will be required.

Another characteristic finding was the conservation of serine and tyrosine residues on KSHV ORF34. At first, the ORF34 serine residue mutant S168A shows a better ability for virus production than ORF34 WT (Fig.4 and 6). Previous studies on vPIC factors among the herpesviruses have shown that multiple serine/threonine residues on EBV BDLF4 (KSHV ORF31 homolog) (41). If phosphorylation occurs on KSHV ORF34, then S168 phosphorylation would be related to the dysregulation of vPIC._Secondly, ORF34 tyrosine residue mutants, Y194A and Y310A, lost their ability to bind to ORF66, L-gene expression and virus release, but they did not lose their ability to bind to ORF18, ORF24, and ORF31 (Fig. 2-6). Thus, the phosphorylation of Y194 and Y310 may be related to the positive regulation of ORF66 binding. However, the prediction model did not indicate the exposure of these residues' side chains to the surface of ORF34 (Fig. 8c). To conclude whether or not phosphorylation on ORF34 occurs, real experimental data are necessary. Not only phosphorylation but also other post-translational modifications may be contributing to vPIC regulation.

Our results demonstrated the importance of the four conserved cysteine residues in the KSHV ORF34 protein for the functional vPIC, following KSHV ORF66 (23, 24). Our evidence and structure prediction suggest that these four cysteines would contribute to cation-capturing, which might be essential for maintaining the conformation of ORF34 as the scaffold for vPIC formation. In addition, we can speculate about the functional possibilities of the character profiling of ORF34 mutants and the predicted structure. The N-terminal domain of ORF34 might be associated with some unknown host factors and bundle multiple vPIC components. Some of the conserved threonine/ serine/ tyrosine residues in ORF34 might be related to the functional regulation of ORF34 by phosphorylation. However, adequate proof has not yet been obtained, and further efforts will be necessary to answer questions concerning this complex.

Material and Methods

Cell culture and reagents

293T cells (RCB2202; RIKEN BioResource Center, Tsukuba, Japan) were cultured in a growth medium. DMEM was supplemented with 10% fetal calf serum and Penicillin-Streptomycin solution (Nacalai Tesque Inc., Kyoto, Japan). The transfection reagent for 293T cells, PEI-MAX MW40000 (Polysciences, Inc., Warrington, PA, USA), was dissolved at a concentration of 1 mg/mL in distilled water and filtered.

Plasmids

pCI-neo-2xS-ORF34 WT, pCI-neo-3xFLAG-ORF66, pCI-neo-3xFLAG-ORF18, and pCI-neo-3xFLAG-ORF31 expression plasmids were previously described (20). Alanine-scanning mutants of ORF34 coding fragments were obtained by PCR or overlap-extension PCR from the KSHV ORF34 expression plasmid using the primer sets indicated in Table 1. To construct pCI-neo-6xMyc-ORF24-BD (1-400), partial ORF24 coding fragments (1-400 a.a.) containing the ORF34 binding region (21) were also obtained by PCR from the KSHV ORF24 expression plasmid. These fragments were cloned into the expression plasmids based on a pCI-neo mammalian expression vector (Promega, Madison, WI, USA), *e.g.* pCI-neo-2xS, pCI-neo-6xMyc, or pCI-blast-3xFLAG.

Establishment of doxycycline-inducible recombinant KSHV-expressing cells and stably ORF34 WT- and mutant-expressing cells

For maintenance, iSLK cells were cultured in growth medium of DMEM/fetal calf serum 10% containing 1 μg/mL puromycin (Fujifilm-Wako Chemicals, Osaka, Japan) and 0.25 mg/mL of G418 (Fujifilm-Wako Chemicals). KSHV BAC16 mutant (ΔORF34-BAC16) and its revertant (ΔORF34Rev-BAC16), as previously described (20), were transfected to iSLK cells using

Screenfect A plus (Fujifilm-Wako Chemicals) according to the manufacturer's instructions. Transfected cells were selected under 1000 μg/mL of hygromycin B (Fujifilm-Wako Chemicals) to establish doxycycline-inducible recombinant KSHV-producing cell lines (iSLK-Δ34Rev and iSLK-Δ34).

To establish stable ORF34-expressing cells for complementation, pCI-blast-3xFLAG-ORF34 and empty vector pCI-blast-3xFLAG were transfected into iSLK-Δ34Rev and iSLK-Δ34 cells, and transfected cells were selected and maintained in 10 μg/mL and 7.5 μg/mL of Blasticidin S (Fujifilm-Wako Chemicals), respectively. Thus, the stable cell lines iSLK-Δ34Rev/pCI-blast-3xFLAG, iSLK-Δ34/pCI-blast-3xFLAG, iSLK-Δ34/pCI-blast-3xFLAG-ORF34WT, and iSLK-Δ34/pCI-blast-3xFLAG-ORF34 mutants were established.

Measurement of KSHV production

For quantification of virus production, KSHV virions in culture supernatant were quantified as described previously (20, 23, 42, 43) with minor modification. In brief, iSLK-harboring KSHV BAC cells were treated with 0.75 mM of NaB and 4 μg/mL of doxycycline for 72 h to induce lytic replication and production of recombinant KSHV, and culture supernatants were harvested. Culture supernatants (150 μL) were treated with DNase I (NEB, Ipswich, MA, USA) to obtain only enveloped and encapsidated viral genomes. Viral DNA was purified and extracted from 100 μL of DNase I-treated culture supernatant using the QIAamp DNA blood mini kit (QIAGEN GmbH, Hilden, Germany). To quantify viral DNA copies, SYBR green real-time PCR was performed using THUNDERBIRD Next SYBR qPCR Mix (TOYOBO, Osaka, Japan) with KSHV-encoded ORF11 specific primers (20, 23).

Quantification of viral gene expression

To assess the roles of ORF34 WT and its mutants in viral gene expression, RT-qPCR was

performed as described previously (23). iSLK-Δ34 cells complemented with ORF34 WT or its mutants were stimulated and cultured as in the previous section. Total RNA was extracted from the treated cell lines using Sepasol-RNA II super (Nacalai Tesque Inc.). Total RNA was digested with DNase by the ReverTra Ace qPCR RT Master Mix with gDNA Remover (TOYOBO) to exclude the host and viral genomic DNA (gDNA), which interfere with the mRNA quantification as a background. cDNA was synthesized using the same kit and subjected to SYBR green real-time PCR using THUNDERBIRD Next SYBR qPCR Mix (TOYOBO) and the primer sets noted in Table 1, based on Fakhari and Dittmer (44) and the selected unique CDS referenced by Bruce *et al.* (45). Relative KSHV mRNA expression was determined by the GAPDH expression and ΔΔCt methods.

Western blotting, pull-down assays, and antibodies

To detect viral proteins, iSLK-Δ34 cells complemented with ORF34 WT or mutants were stimulated and cultured as in the previous section. Treated cells were washed with PBS, directly lysed with WB sample buffer, and boiled. The WB samples were then subjected to Western blotting as described previously (23).

Pull-down assays between the vPIC components and ORF34 were performed as described previously (20, 23, 28). In brief, 293T cells were transfected with the indicated plasmids using PEI-MAX (46) and cultured for two days. Transfected cells were lysed by Lysis buffer (20 mM HEPES (pH 7.9), 0.18 M NaCl, 0.1% (v/v) NP-40, 10% (v/v) Glycerol, 0.1 mM EDTA) with protease inhibitors and briefly sonicated to destroy the cell nucleus. Whole-cell extract, which is the supernatant obtained from the lysate centrifuged to discard cell debris, was subjected to affinity purification using S-protein-agarose (Merck Millipore, Burlington, MA, USA) for one to two hours and washed four times. Purified precipitates, including bait and prey proteins (2xS-tagged ORF34 WT/mutants and its counterparts) binding to S-protein-

agarose, and whole-cell extracts were subjected to Western blotting.

Treatment of the vPIC interaction with the zinc chelator TPEN (*N*,*N*,*N′*,*N′*-Tetrakis (2-pyridylmethyl) ethylenediamine; TCI, Tokyo, Japan) was also performed as described previously (23). In brief, 293T cell lysate transfected with 2xS-ORF34 or control vector was subjected to S-protein-agarose purification in the presence of each dose of TPEN or vehicle (ethanol). The beads associated with bait protein ORF34 WT or control were mixed with the cell lysate of prey proteins (6xMyc-ORF24BD or 3xFLAG-ORF66) and overexpressed in 293T cells in the presence of each dose of TPEN or vehicle. The beads were washed four times and subjected to Western blotting.

Anti-Myc (9E10; Santa-Cruz, CA, USA), Anti-S-tag pAb (MBL, Nagoya, Japan), Anti-FLAG (DDDDK-tag) (FLA-1; MBL), Anti-HHV8 K-bZIP (F33P1; Santa-Cruz), Anti-HHV8 K8.1A/B (4A4; Santa-Cruz), and Anti-β-Tubulin (10G10; Fujifilm-Wako Chemicals) were used as the primary antibodies. HRP-linked anti-mouse IgG antibody (Jackson ImmunoResearch, Inc., West Grove, PA, USA) and HRP-linked anti-rabbit IgG antibody (Jackson ImmunoResearch, Inc.) were used as the secondary antibodies. Antibody-bound proteins were visualized with ECL Western Blotting Detection Reagents (ATTO, Tokyo, Japan) on X-ray film (FUJIFILM Corp., Tokyo, Japan).

The pull-down efficiency score indicates that the band intensity of the prey protein (ORF24BD, ORF66) obtained from the mean region of interest using the ImageJ software program (Version; 2.0.0-rc-43/1.52n) was normalized by that of the bait protein (ORF34 WT/mutants).

Statistical analyses and data visualization

The standard deviation was determined by analyzing the data obtained from three to four independent samples and is indicated as the error bars. The two-tailed Student's *t*-test was used

to specify the differences between the indicated groups. *P* values are shown in each figure. For the functional profile analysis of ORF34 WT and its mutants, a heatmap with a dendrogram that highlights the hierarchical clustering was visualized using R (Ver 4.0.3) and R Studio with R package “Superheat” (https://rlbarter.github.io/superheat/)(47).

Protein structure prediction and ion binding prediction and modeling

The KSHV ORF34 protein structure model was predicted using the AlphaFold 2.2.0 software program (https://github.com/deepmind/alphafold) in the local environment (29). The following databases were utilized for AlphaFold2: Uniclust30 (version 2018_08), MGnify (version 2018_12), pdb70 (downloaded on Feb 15th, 2022), PDB/mmCIF (downloaded on Feb 18th, 2022), and pdb_seqres (downloaded on Feb 18th, 2022). Of note, several versions or frequently updated versions of these databases were utilized. The predicted model was visualized with the molecular visualization open-source software program PyMOL (Ver 2.5.0). In addition, the pLDDT score coloring of the predicted model was visualized with the python module "PSICO" (https://github.com/speleo3/pymol-psico). The visualization of the PAE plot was completed using the python module "plddt2csv" (https://github.com/CYP152N1/plddt2csv). For predicting disordered protein regions of KSHV ORF34, PrDOS (https://prdos.hgc.jp/cgi-bin/top.cgi) and DISOPRED3 (http://bioinf.cs.ucl.ac.uk/psipred) were also used (38, 39).

The metal ion-binding (MIB) site prediction and modeling server (http://bioinfo.cmu.edu.tw/MIB/) was used to predict the binding residues of 18 different metal ions (Ca^{2+}, Cu^{+}, Cu^{2+}, Fe^{2+}, Fe^{3+}, Mg^{2+}, Mn^{2+}, Zn^{2+}, Cd^{2+}, Ni^{2+}, Hg^{2+}, Co^{2+}, Au^{+}, Ba^{2+}, Pb^{2+}, Pt^{2+}, Sm^{3+}, and Sr^{2+}) in a protein (30, 48). The query of the protein structure was compared to metal-ion binding templates, which allowed MIB residues within at least 3.5 Å of the ion to be predicted, along with a binding score and template. The template with the highest binding score over 3.0 was documented if the same binding residue was present multiple times for a single metal ion.

Acknowledgments

BAC16, a KSHV BAC clone, was a kind gift from Dr. Jae U Jung (Lerner Research Institute of Cleveland Clinic, USA). We also thank Dr. Gregory A. Smith (Northwestern Univ., USA) for providing the *E. coli* strain GS1783.

This work was partially supported by a Grant-in-Aid for Scientific Research (C) (21K08509; T.W., and 19K07669; S.O.), Takeda Science Foundation (T.W.), The Association for Research on Lactic Acid Bacteria (S.O.), the University of the Ryukyus Research Project Promotion Grant for Young Researchers (20SP04102; T.W.), the research start-up from Saint Joseph's University (250114-214010-7351; T.I.), and the National Institutes of Health through a grant from the National Institute of Allergy and Infectious Diseases (R15AI172610; T.I.).

Figure legends

Fig. 1. Conserved amino-acid residues of ORF34 homolog and alanine-scanning mutants. Amino acid sequence alignment of KSHV ORF34. Herpesvirus homolog amino acid sequences were translated from nucleotide sequences found in the NCBI database (KSHV ORF66 (JSC-1-BAC16; Accession number GQ994935), MHV68 ORF34 (strain WUMS; NC_001826), EBV BGLF3 (strain B95-8; V01555), CMV UL95 (strain Towne; FJ616285), HHV6B U67 (strain japan-a1; KY239023)). Raw data regarding alignment were obtained using Clustal Omega (EMBL-EBI; https://www.ebi.ac.uk/Tools/msa/clustalo/). Completely conserved amino acids between homologs are indicated by a gray background. Based on the alignment information, 1-2 conserved amino acids residues, except for proline and alanine, were substituted with alanine for ORF34 alanine-scanning mutants, as depicted.

Fig. 2. Physical interactions between ORF34 alanine-scanning mutants and vPIC components, ORF24 and ORF66. 293T cells were co-transfected with expression plasmids of the 2xS-ORF34 alanine-scanning mutant and 6xMyc-ORF24BD (a-c) or 3xFLAG-ORF66 (d-f). ORF24BD corresponds to the KSHV ORF24 N-terminal domain (1-400 a.a.) reported as having a domain interaction with ORF34 (21). Transfected cells were lysed, and cell lysates were subjected to pull-down assays using S-protein-agarose that captured the 2xS-ORF34 mutants. Obtained precipitates including 2xS-ORF34 mutants were probed with indicated antibodies to detect interactions. The pull-down efficiency score of each interaction was indicated below the pull-down panel of prey proteins (6xMyc-ORF24BD or 3xFLAG-ORF66). The pull-down efficiency score of the sample co-transfected with ORF34 WT and ORF24BD/ORF66 was defined as 1.0. N.D. (not detected) indicates that a positive signal of the prey proteins was not detected.

Fig. 3. Physical interaction between ORF34 alanine-scanning mutants and vPIC components, ORF18 and ORF31. 293T cells were co-transfected with expression plasmids of 2xS-ORF34 alanine-scanning mutant and 3xFLAG-ORF18 (a-c) or 3xFLAG-ORF31 (d-f). Transfected cells were lysed and cell lysates were subjected to pull-down assays using S-protein-agarose that captured the 2xS-ORF34 mutants. Obtained precipitates including 2xS-ORF34 mutants were probed with the indicated antibodies to detect interactions.

Fig. 4. Complement abilities of ORF34 alanine-scanning mutants on viral production. Establishment of 3xFLAG-tagged ORF34-expressing iSLK-Δ34 stable cell lines and confirmation of the recovery by ORF34 WT in ΔORF34-virus production. (a) The Western blot showed exogenous 3xFLAG-tagged ORF34 WT expression in iSLK-Δ34 cells. (b) A complementation assay was performed to rescue virus production. (c-e) 3xFLAG-tagged ORF34 alanine-scanning mutant-expressing iSLK-Δ34 stable cell lines were investigated for their virus production recoveries, with results shown in the upper graph panels. The lower blot panels indicate the exogenous ORF34 WT/mutant expression under normal culture conditions. In the upper graph panels, the virus production of iSLK-Δ34/ORF34 WT cells was defined as 100%. Each stable iSLK-KSHV BAC-harboring cell line was activated by NaB (0.75 mM) and Dox (4 μG/mL) and cultured for 3 days, and the culture supernatant containing encapsidated KSHV genome was harvested and quantified. Three independent samples were evaluated by real-time PCR and indicated as dots in each column. The error bars indicate standard deviations.

Fig. 5. Complement abilities of ORF34 alanine-scanning mutants for viral gene transcription and protein expression. The mRNA and protein expression in lytic-induced iSLK-Δ34 cells complemented with ORF34 WT/alanine-scanning mutants. The cells were cultured for three days in conditioned medium containing NaB and Dox to induce a lytic state.

(a-c) Total RNA was extracted from cells and subjected to RT-qPCR. The mRNA expression of viral genes, which is representative of each step (K4 as IE gene, ORF6 as E gene, K8.1 as L-gene), was normalized by GAPDH expression. The mRNA expression of iSLK-ΔORF34/Control cells was defined as 1.0. Four independent samples were evaluated and indicated as dots in each column. The error bars indicate standard deviations. (d-e) Total protein samples were prepared from each lytic-induced cell and subjected to Western blotting. The protein expression of the L-gene was analyzed by K8.1A/B blotting and the E gene by K-bZIP, respectively. The protein expression score, the band intensity, of iSLK-Δ34/ORF34 WT was defined as 1.0. N.D. (not detected), indicating that a positive signal of viral proteins was not detected.

Fig. 6. Summary of the effects of ORF34 alanine-scanning mutants on the vPIC function. The results (Fig. 2, 4-5) were summarized and visualized on the heatmap with a dendrogram highlighting the hierarchical clustering. Each score of ORF34 WT or iSLK-Δ34/WT was defined as 1.0. The scores are indicated on each panel with the color gradient (dark blue [0.0] - green [1.0] - yellow [>3.0]) as indicated by the lower bar. N.D. (not detected) in each experiment is indicated by the gray panel. Groups were classified according to the visualized dendrogram.

Fig. 7. ORF34 structure model predicted by Alphafold2 and conserved cysteines on ORF34. The ORF34 structure was predicted, and conserved cysteines on the model were highlighted. (a) ORF34 structure prediction using the deep-learning algorithm Alphafold2. The illustration depicts the protein labeled with colors according to the pLDDT score of each amino-acid residue (left panel). The region of the conserved cysteines is enclosed, and the side chains of the cysteines are labeled with green (center panel). Sulfur atoms of the cysteines on

the stick are labeled with dark yellow (right panel). (b) The 2D plot of the pLDDT score and amino-acid residues on ORF34 (1-327 a.a.), emphasizing the conserved amino-acid residues. (c) Prediction alignment error (PAE) plot of the predicted ORF34 structure. Each dot indicates the predicted distance between amino-acid residues.

Fig. 8. Overview of the predicted ORF34 structure and mutated residues. (a) Rotated ORF34 structures predicted by AlphaFold2. The illustration model is labeled with colors according to the pLDDT score. (b-c) While the conserved cysteines are labeled with green, other mutated amino-acid residues are highlighted with magenta in the illustration model (b) and the surface-illustration model (c).

Fig. 9. The prediction of metal cation binding to ORF34 and its influence on the binding ability of ORF34. (a) The table organizes the binding residues, templates, and binding scores of 18 different metal ions predicted by the Metal Ion-Binding site prediction and modeling server, MIB2. When multiple copies of identical binding residues were present for a single metal ion, the template with the highest binding score was noted. If any new binding residues were present amongst previously recorded ones, the template was still recorded. Prediction binding scores higher than 3.0 are listed. Conserved cysteine residues (C170, C175, C256, C256) were highlighted with magenta. (b) Predicted model of ORF34 structure binding to ions. The illustration model of ORF34 was visualized according to Fig. 7a (right panel), and the binding zinc ion (Zn^{2+}) is shown as a gray sphere. Heavy metal cation chelation influences the ORF34 binding abilities to ORF24BD (c) and ORF66 (d). Pull-down assays using S-tagged ORF34 binding beads as bait in the presence of cell extracts overexpressed prey proteins (6xMyc-ORF24BD or 3xFLAG-ORF66) and the heavy metal chelator TPEN. The pull-down efficiency score is indicated below the pull-down panel of the prey protein. The score of the

1 sample co-incubated with 2xS-ORF34 WT binding beads as bait and 6xMyc-ORF24BD or

2 3xFLAG-ORF66 as prey was defined as 1.0.

3

References

1. Damania BA, Cesarman E. 2022. Kaposi's Sarcoma Herpesvirus, p 513-572. *In* Knipe DM, Howley PM, Damania BA, Cohen JI (ed), Fields Virology, 7th Edition, vol 2. Lippincott Williams & Wilkins.
2. Cesarman E, Chadburn A, Rubinstein PG. 2022. KSHV/HHV8-mediated hematologic diseases. Blood 139:1013-1025.
3. Wen KW, Wang L, Menke JR, Damania B. 2021. Cancers associated with human gammaherpesviruses. FEBS J doi:10.1111/febs.16206.
4. Wen KW, Damania B. 2010. Kaposi sarcoma-associated herpesvirus (KSHV): molecular biology and oncogenesis. Cancer Lett 289:140-50.
5. Cesarman E, Damania B, Krown SE, Martin J, Bower M, Whitby D. 2019. Kaposi sarcoma. Nat Rev Dis Primers 5:9.
6. Krug LT, Pellet PE. 2022. The family Herpesviridae: A Brief introduction, p 212-234. *In* Knipe DM, Howley PM, Damania BA, Cohen JI (ed), Fields Virology, 7th Edition, vol 2. Lippincott Williams & Wilkins.
7. Pellett PE, Davison, A.J., Eberle, R., Ehlers, B., Hayward, G.S., Lacoste, V., Minson, A.C., Nicholas, J., Roizman, B., Studdert, M.J. and Wang, F. 2011. Order *Herpesvirales*. *In* King A, Lefkowitz E., Adams, M.J., Carstens, E.B. (ed), Virus Taxonomy: Ninth Report of the International Committee on Taxonomy of Viruses. Elsevier.
8. Pellett PE, Davison, A.J., Eberle, R., Ehlers, B., Hayward, G.S., Lacoste, V., Minson, A.C., Nicholas, J., Roizman, B., Studdert, M.J., Wang, F. 2011. Family *Herpesviridae*, p 81-92. *In* King A, Lefkowitz E., Adams, M.J., Carstens, E.B. (ed), Virus Taxonomy: Ninth Report of the International Committee on Taxonomy of Viruses. Elsevier.
9. Gewurz BE, Longnecker RM, Cohen JI. 2022. Epstein-Barr Virus, p 324-388. *In* Knipe DM, Howley PM, Damania BA, Cohen JI (ed), Fields Virology, 7th Edition, vol 2. Lippincott Williams & Wilkins.
10. Cohen JI. 2020. Herpesvirus latency. J Clin Invest 130:3361-3369.
11. Gunther T, Grundhoff A. 2010. The epigenetic landscape of latent Kaposi sarcoma-associated herpesvirus genomes. PLoS Pathog 6:e1000935.
12. Toth Z, Maglinte DT, Lee SH, Lee HR, Wong LY, Brulois KF, Lee S, Buckley JD, Laird PW, Marquez VE, Jung JU. 2010. Epigenetic analysis of KSHV latent and lytic genomes. PLoS Pathog 6:e1001013.
13. Toth Z, Brulois K, Jung JU. 2013. The chromatin landscape of Kaposi's sarcoma-associated herpesvirus. Viruses 5:1346-73.
14. Jenner RG, Alba MM, Boshoff C, Kellam P. 2001. Kaposi's sarcoma-associated herpesvirus latent and lytic gene expression as revealed by DNA arrays. J Virol

75:891-902.
15. Guito J, Lukac DM. 2012. KSHV Rta Promoter Specification and Viral Reactivation. Front Microbiol 3:30.
16. Miller G, El - Guindy A, Countryman J, Ye J, Gradoville L. 2007. Lytic Cycle Switches of Oncogenic Human Gammaherpesviruses1, p 81-109 doi:10.1016/s0065-230x(06)97004-3.
17. Sun R, Lin SF, Gradoville L, Yuan Y, Zhu F, Miller G. 1998. A viral gene that activates lytic cycle expression of Kaposi's sarcoma-associated herpesvirus. Proc Natl Acad Sci U S A 95:10866-71.
18. Hancock MH, Skalsky RL. 2018. Roles of Non-coding RNAs During Herpesvirus Infection. Curr Top Microbiol Immunol 419:243-280.
19. Gruffat H, Marchione R, Manet E. 2016. Herpesvirus Late Gene Expression: A Viral-Specific Pre-initiation Complex Is Key. Front Microbiol 7.
20. Nishimura M, Watanabe T, Yagi S, Yamanaka T, Fujimuro M. 2017. Kaposi's sarcoma-associated herpesvirus ORF34 is essential for late gene expression and virus production. Sci Rep 7:329.
21. Davis ZH, Hesser C, Park J, Glaunsinger BA. 2015. Interaction Between ORF24 and ORF34 in the Kaposi's Sarcoma-Associated Herpesvirus Late Gene Transcription Factor Complex is Essential For Viral Late Gene Expression. J Virol doi:10.1128/jvi.02157-15.
22. Brulois K, Wong LY, Lee HR, Sivadas P, Ensser A, Feng P, Gao SJ, Toth Z, Jung JU. 2015. Association of Kaposi's Sarcoma-Associated Herpesvirus ORF31 with ORF34 and ORF24 Is Critical for Late Gene Expression. J Virol 89:6148-54.
23. Watanabe T, Nishimura M, Izumi T, Kuriyama K, Iwaisako Y, Hosokawa K, Takaori-Kondo A, Fujimuro M. 2020. Kaposi's Sarcoma-Associated Herpesvirus ORF66 Is Essential for Late Gene Expression and Virus Production via Interaction with ORF34. J Virol 94.
24. Didychuk AL, Castaneda AF, Kushnir LO, Huang CJ, Glaunsinger BA. 2020. Conserved CxnC Motifs in Kaposi's Sarcoma-Associated Herpesvirus ORF66 Are Required for Viral Late Gene Expression and Are Essential for Its Interaction with ORF34. J Virol 94.
25. Gong D, Wu NC, Xie Y, Feng J, Tong L, Brulois KF, Luan H, Du Y, Jung JU, Wang CY, Kang MK, Park NH, Sun R, Wu TT. 2014. Kaposi's sarcoma-associated herpesvirus ORF18 and ORF30 are essential for late gene expression during lytic replication. J Virol 88:11369-82.
26. Castañeda AF, Glaunsinger BA. 2019. The Interaction between ORF18 and ORF30 Is Required for Late Gene Expression in Kaposi's Sarcoma-Associated Herpesvirus. J Virol 93:e01488-18.

27. Davis Zoe H, Verschueren E, Jang Gwendolyn M, Kleffman K, Johnson Jeffrey R, Park J, Von Dollen J, Maher MC, Johnson T, Newton W, Jäger S, Shales M, Horner J, Hernandez Ryan D, Krogan Nevan J, Glaunsinger Britt A. 2015. Global Mapping of Herpesvirus-Host Protein Complexes Reveals a Transcription Strategy for Late Genes. Mol Cell 57:349-360.
28. Maeda Y, Watanabe T, Izumi T, Kuriyama K, Ohno S, Fujimuro M. 2022. Biomolecular Fluorescence Complementation Profiling and Artificial Intelligence Structure Prediction of the Kaposi’s Sarcoma-Associated Herpesvirus ORF18 and ORF30 Interaction. Int J Mol Sci 23:9647.
29. Jumper J, Evans R, Pritzel A, Green T, Figurnov M, Ronneberger O, Tunyasuvunakool K, Bates R, Zidek A, Potapenko A, Bridgland A, Meyer C, Kohl SAA, Ballard AJ, Cowie A, Romera-Paredes B, Nikolov S, Jain R, Adler J, Back T, Petersen S, Reiman D, Clancy E, Zielinski M, Steinegger M, Pacholska M, Berghammer T, Bodenstein S, Silver D, Vinyals O, Senior AW, Kavukcuoglu K, Kohli P, Hassabis D. 2021. Highly accurate protein structure prediction with AlphaFold. Nature 596:583-589.
30. Lu C-H, Chen C-C, Yu C-S, Liu Y-Y, Liu J-J, Wei S-T, Lin Y-F. 2022. MIB2: metal ion-binding site prediction and modeling server. Bioinformatics 38:4428-4429.
31. Wehrspan ZJ, McDonnell RT, Elcock AH. 2022. Identification of Iron-Sulfur (Fe-S) Cluster and Zinc (Zn) Binding Sites Within Proteomes Predicted by DeepMind's AlphaFold2 Program Dramatically Expands the Metalloproteome. J Mol Biol 434:167377.
32. Okuda M, Tanaka A, Arai Y, Satoh M, Okamura H, Nagadoi A, Hanaoka F, Ohkuma Y, Nishimura Y. 2004. A novel zinc finger structure in the large subunit of human general transcription factor TFIIE. J Biol Chem 279:51395-403.
33. Chen HT, Legault P, Glushka J, Omichinski JG, Scott RA. 2000. Structure of a (Cys3His) zinc ribbon, a ubiquitous motif in archaeal and eucaryal transcription. Protein Sci 9:1743-52.
34. Qian X, Jeon C, Yoon H, Agarwal K, Weiss MA. 1993. Structure of a new nucleic-acid-binding motif in eukaryotic transcriptional elongation factor TFIIS. Nature 365:277-279.
35. Wang B, Jones DN, Kaine BP, Weiss MA. 1998. High-resolution structure of an archaeal zinc ribbon defines a general architectural motif in eukaryotic RNA polymerases. Structure 6:555-69.
36. Okuda M, Tanaka A, Hanaoka F, Ohkuma Y, Nishimura Y. 2005. Structural insights into the asymmetric effects of zinc-ligand cysteine mutations in the novel zinc ribbon domain of human TFIIEalpha for transcription. J Biochem

138:443-9.
37. Ghosh M, Elsby LM, Mal TK, Gooding JM, Roberts SG, Ikura M. 2004. Probing Zn2+-binding effects on the zinc-ribbon domain of human general transcription factor TFIIB. Biochem J 378:317-24.
38. Ishida T, Kinoshita K. 2007. PrDOS: prediction of disordered protein regions from amino acid sequence. Nucleic Acids Res 35:W460-4.
39. Jones DT, Cozzetto D. 2015. DISOPRED3: precise disordered region predictions with annotated protein-binding activity. Bioinformatics 31:857-63.
40. Li J, Walsh A, Lam TT, Delecluse HJ, El-Guindy A. 2019. A single phosphoacceptor residue in BGLF3 is essential for transcription of Epstein-Barr virus late genes. PLoS Pathog 15:e1007980.
41. Sato Y, Watanabe T, Suzuki C, Abe Y, Masud H, Inagaki T, Yoshida M, Suzuki T, Goshima F, Adachi J, Tomonaga T, Murata T, Kimura H. 2019. S-Like-Phase Cyclin-Dependent Kinases Stabilize the Epstein-Barr Virus BDLF4 Protein To Temporally Control Late Gene Transcription. J Virol 93.
42. Wakao K, Watanabe T, Takadama T, Ui S, Shigemi Z, Kagawa H, Higashi C, Ohga R, Taira T, Fujimuro M. 2014. Sangivamycin induces apoptosis by suppressing Erk signaling in primary effusion lymphoma cells. Biochem Biophys Res Commun 444:135-40.
43. Watanabe T, Nakamura S, Ono T, Ui S, Yagi S, Kagawa H, Watanabe H, Ohe T, Mashino T, Fujimuro M. 2014. Pyrrolidinium fullerene induces apoptosis by activation of procaspase-9 via suppression of Akt in primary effusion lymphoma. Biochem Biophys Res Commun 451:93-100.
44. Fakhari FD, Dittmer DP. 2002. Charting Latency Transcripts in Kaposi's Sarcoma-Associated Herpesvirus by Whole-Genome Real-Time Quantitative PCR. J Virol 76:6213-6223.
45. Bruce AG, Barcy S, DiMaio T, Gan E, Garrigues HJ, Lagunoff M, Rose TM. 2017. Quantitative Analysis of the KSHV Transcriptome Following Primary Infection of Blood and Lymphatic Endothelial Cells. Pathogens (Basel, Switzerland) 6:11.
46. Katoh Y, Nozaki S, Hartanto D, Miyano R, Nakayama K. 2015. Architectures of multisubunit complexes revealed by a visible immunoprecipitation assay using fluorescent fusion proteins. J Cell Sci 128:2351-62.
47. Barter RL, Yu B. 2018. Superheat: An R package for creating beautiful and extendable heatmaps for visualizing complex data. J Comput Graph Stat 27:910-922.
48. Lu CH, Lin YF, Lin JJ, Yu CS. 2012. Prediction of metal ion-binding sites in proteins using the fragment transformation method. PLoS One 7:e39252.

1

2

Fig.1

```
KSHV_ORF34   0   ------------------------------------------------------------ 0
MHV68_ORF34  0   ------------------------------------------------------------ 0
EBV_BGLF3    0   ------------------------------------------------------------ 0
HCMV_UL95    60  MMAAAVVRAEVRRQRREERKKMAAARTTEDPPENHVVADVACGTGAVTRSSSSSLVVSSS 60
HHV6B_U67    0   ------------------------------------------------------------ 0

KSHV_ORF34   1   ----------------------------------------MFALSSLVSEGDP---EV 15
MHV68_ORF34  1   ----------------------------------------MATLSDFFPEADP---VL 15
EBV_BGLF3    1   ----------------------------------------MFNAVKADMPDDP---ML 15
HCMV_UL95    61  SASGSDEPSSASPLSFPVCSPSTAVRSPGSAGVSTSLCSVERMVELS-AQSPAADFSVSE 120
HHV6B_U67    1   ------------------------------MWVMSQVRSMEPDLTLAAVYQAAANLTEQD 30

                                                E41A/T42A  F47A V50A
KSHV_ORF34   16  TSRYVKGVQLALDLSENT--PGQFKLIETPLNSFLLVSNVMPEVQPIC-SGRP---AL-- 67
MHV68_ORF34  16  EKNYRRCVDLAINMSWSV--PGQFKLVETPINSFLLVGDVLPNDMI---ESKP---VN-- 65
EBV_BGLF3    16  ARRYGQCLELALEACQDT--PEQFKLVETPLKSFLLVSNILPQDNRPWHEARS---SGRV 70
HCMV_UL95    121 AWRFEEAVNMALVACEAVSPYDRFRLIETPDENFLLVTNVIPRESAEVPVLDSSSSGGDS 180
HHV6B_U67    31  KEIFSEAVKTAFSVCSSAAPSARLRMIETPTQNFMFVTSVIPSGVPS------------ 77

KSHV_ORF34   68  ---RPDFSNLHLPRL------------------E----K-----LQRVLGQGFGAAGEE- 96
MHV68_ORF34  66  ---STNLVNIPFPLS------------------T----LGVSTSKKSVEVTSYKSETEK- 99
EBV_BGLF3    71  AEDDYDFSSLALELL------------------P----LNPRL----PEEWQFGGQGWS- 103
HCMV_UL95    181 GPEDK-KKNVGNKTAGEKNGGGSRAKRRRRRRAPKNDAATPSFLRRHDVLERFAAAAEPL 239
HHV6B_U67    78  GEKKT-KLNIDAAL---D------------------NLALSF-------------ANKK 101

KSHV_ORF34   97  ---------IALDPSHVETHEKGQVFYNHYATEEWTWALTLNKDALLREAVDGLCDPGTW 147
MHV68_ORF34  100 ---------FQEAASISEHSIRGSIV---YEGLTWITAMGYNVTDFLVNMLEQMKCPENW 147
EBV_BGLF3    104 ---------SRMEPSQPE--MGMGLCFEVFDGDLMRIALAWNKDEVIGQALQILAHSQTW 152
HCMV_UL95    240 PSLCVRDYALRNADRVTYDGELIYGSYLLYRKAHVELSLSSNKVQHVEAVLRQVYTPGLL 299
HHV6B_U67    102 SKKMARTYLLQNVSRTQDQQVAISGTYILYTKKHIETSLMLDKTKLVKQILEYAETPNLL 161

                 D154A  W160A  G165A S168A C170A  C175A   G182A  L188A/L189A Y194A
KSHV_ORF34   148 KGLLPDDPLPLLWLLFNGPASFCRADCCLYKQHCG--YPGPVLLPGHMYAPKRDLLSFVN 205
MHV68_ORF34  148 SGLHPVDPLACVWLLYFGPKSRCSEIACVSELFIG--KKGPILLPPHMYRGDTSVNSFAH 205
EBV_BGLF3    153 TSLVPEDPLPWMWALFYGPRSHCEERHCVYAAARG--KRGPILLPTAVYTPCANIEAFLA 210
HCMV_UL95    300 DHHNVCDVEALLWLLYCGPRSFCARDTCFGREKNG--CPFPALLPKLFYEPVRDYMTYMN 357
HHV6B_U67    162 GYTDVRDLECLLWLVFCGPKSFCQSDSCFGYSKTGYNAAFPNLLPPYLYECGQNNGLFFG 201

                 Y215A
KSHV_ORF34   206 HALKYTKFLYGDFSGTWAAAC-------------R-----------------------PP 229
MHV68_ORF34  206 HLCQYVKHLYADYEPEIL----------------S-----------------------CP 226
EBV_BGLF3    211 HLTRCVYALYLDVRDWKGEDI-------------A-----------------------PP 234
HCMV_UL95    358 LAELYVFVWYRGYEFPAPTPQATTAGSGGGGGAGACAVETSASAGRVDDAGDEVHLPLKP 417
HHV6B_U67    202 IVQAYVFSWYSDFDFSALEIS-----------------------------------------E 223

                 R234A                                C256A  C259A  Q264A/N265A
KSHV_ORF34   230 FATSRIQRVVSQMKIIDA-----SDTYISHTCLLCHIYQQNSI--I--AG--QGTHVGGI 278
MHV68_ORF34  227 LDITRVKGCLSDLRQVAE-----SCVFLSQRCLLCHLYKQNAA--V--SK--NILTASDC 275
EBV_BGLF3    235 FDVSRLNKMAKQLCLLPQ-----EPFCITRVCLLCLLHKQNLNAQY--KR--PVDTYDPC 285
HCMV_UL95    418 VSLDRLREVLQAVRGRFSGREVPAWPASSRTCLLCALYSQNRLCLDLARDEARTVSYSPI 477
HHV6B_U67    224 RARRRIRSLLYDLKQKFSEQEISVLPVASQMCIFCALYKQNKLSLEYVSGDLKTSVFSPI 283

                                                Y310A
KSHV_ORF34   279 LLLSGKGTQYITGNVQTQRCPTTGDYLIIPSYDIPAIITMIKENGLNQL-------- 327
MHV68_ORF34  276 IILGGSGKSLLGTYMKSYKDPATHDSILLPTYNLEAIVNYILEHYGHETAGQEINWE 332
EBV_BGLF3    286 LILTGEAERYMVDAVGNYREASTGTTVLYPTYDLGSIVADMVTYEDE---------- 332
HCMV_UL95    478 VIQDC--AAAVTDVTLSHILPGQSTVSLFPVYHVGKLLDALSLNDAGLITLNL---- 528
HHV6B_U67    284 IIKDC--LCVQTTISTTQMLPGTKSSAIFPVYDLRKLLSALVISEGSV-RFDI---- 333
```

Fig.2

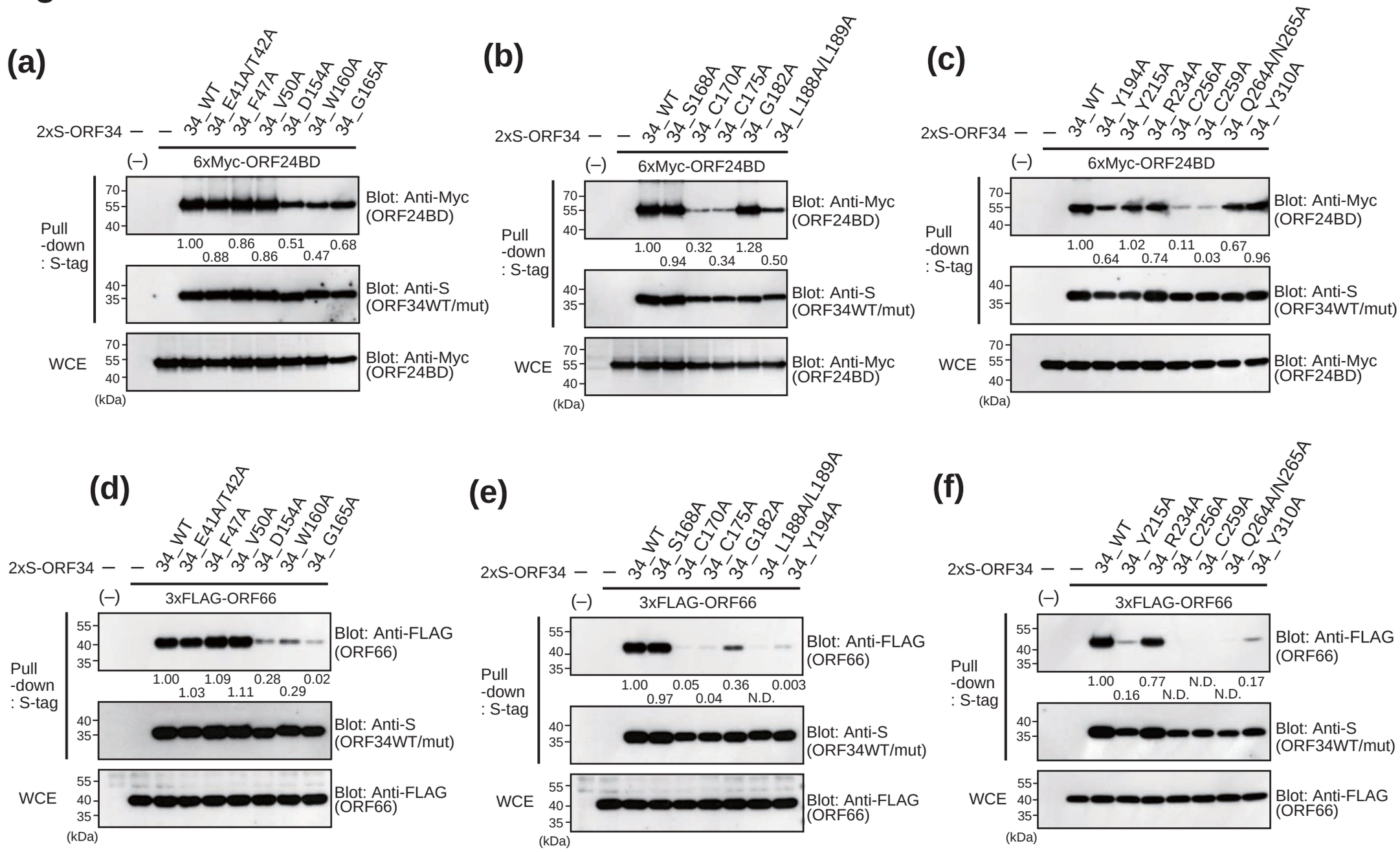
(a)
2xS-ORF34
34_WT
34_E41A/T42A
34_F47A
34_V50A
34_D154A
34_W160A
34_G165A
(–)
6xMyc-ORF24BD
Pull-down : S-tag
Blot: Anti-Myc (ORF24BD)
1.00 0.86 0.51 0.68
0.88 0.86 0.47
Blot: Anti-S (ORF34WT/mut)
WCE
Blot: Anti-Myc (ORF24BD)
(kDa)
(b)
34_WT
34_S168A
34_C170A
34_C175A
34_G182A
34_L188A/L189A
1.00 0.32 1.28
0.94 0.34 0.50
(c)
34_Y194A
34_Y215A
34_R234A
34_C256A
34_C259A
34_Q264A/N265A
34_Y310A
1.00 1.02 0.11 0.67
0.64 0.74 0.03 0.96
(d)
3xFLAG-ORF66
Blot: Anti-FLAG (ORF66)
1.00 1.09 0.28 0.02
1.03 1.11 0.29
(e)
1.00 0.05 0.36 0.003
0.97 0.04 N.D.
(f)
1.00 0.77 N.D. 0.17
0.16 N.D. N.D.

Fig.3

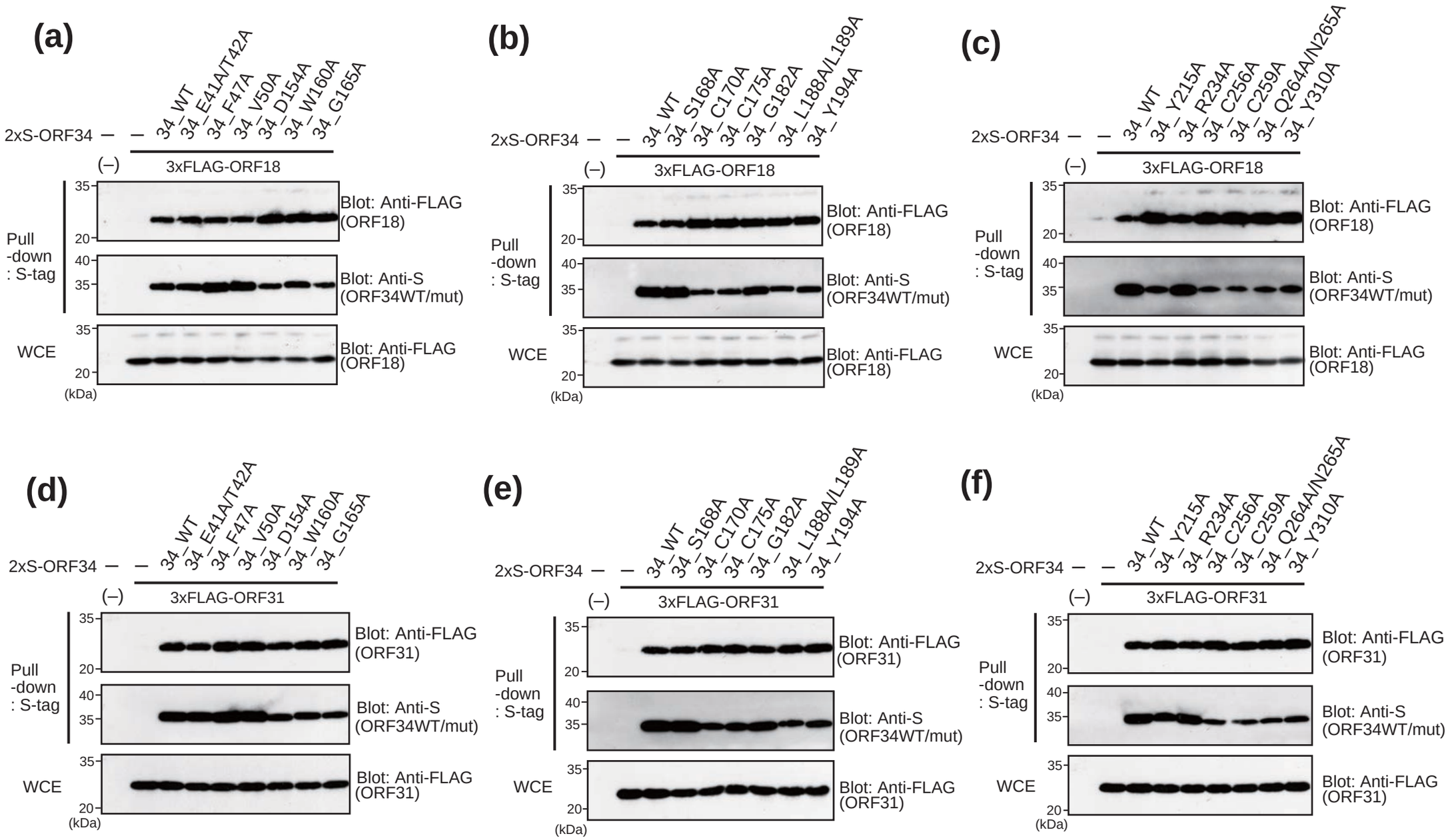
(a)
2xS-ORF34
–
–
34_WT
34_E41A/T42A
34_F47A
34_V50A
34_D154A
34_W160A
34_G165A
(–)
3xFLAG-ORF18
Pull-down : S-tag
WCE
Blot: Anti-FLAG (ORF18)
Blot: Anti-S (ORF34WT/mut)
Blot: Anti-FLAG (ORF18)
35
20
40
35
35
20
(kDa)
(b)
2xS-ORF34
–
–
34_WT
34_S168A
34_C170A
34_C175A
34_G182A
34_L188A/L189A
34_Y194A
(–)
3xFLAG-ORF18
Pull-down : S-tag
WCE
Blot: Anti-FLAG (ORF18)
Blot: Anti-S (ORF34WT/mut)
Blot: Anti-FLAG (ORF18)
35
20
40
35
35
20
(kDa)
(c)
2xS-ORF34
–
–
34_WT
34_Y215A
34_R234A
34_C256A
34_C259A
34_Q264A/N265A
34_Y310A
(–)
3xFLAG-ORF18
Pull-down : S-tag
WCE
Blot: Anti-FLAG (ORF18)
Blot: Anti-S (ORF34WT/mut)
Blot: Anti-FLAG (ORF18)
35
20
40
35
35
20
(kDa)
(d)
2xS-ORF34
–
–
34_WT
34_E41A/T42A
34_F47A
34_V50A
34_D154A
34_W160A
34_G165A
(–)
3xFLAG-ORF31
Pull-down : S-tag
WCE
Blot: Anti-FLAG (ORF31)
Blot: Anti-S (ORF34WT/mut)
Blot: Anti-FLAG (ORF31)
35
20
40
35
35
20
(kDa)
(e)
2xS-ORF34
–
–
34_WT
34_S168A
34_C170A
34_C175A
34_G182A
34_L188A/L189A
34_Y194A
(–)
3xFLAG-ORF31
Pull-down : S-tag
WCE
Blot: Anti-FLAG (ORF31)
Blot: Anti-S (ORF34WT/mut)
Blot: Anti-FLAG (ORF31)
35
20
40
35
35
20
(kDa)
(f)
2xS-ORF34
–
–
34_WT
34_Y215A
34_R234A
34_C256A
34_C259A
34_Q264A/N265A
34_Y310A
(–)
3xFLAG-ORF31
Pull-down : S-tag
WCE
Blot: Anti-FLAG (ORF31)
Blot: Anti-S (ORF34WT/mut)
Blot: Anti-FLAG (ORF31)
35
20
40
35
35
20
(kDa)

Fig.4

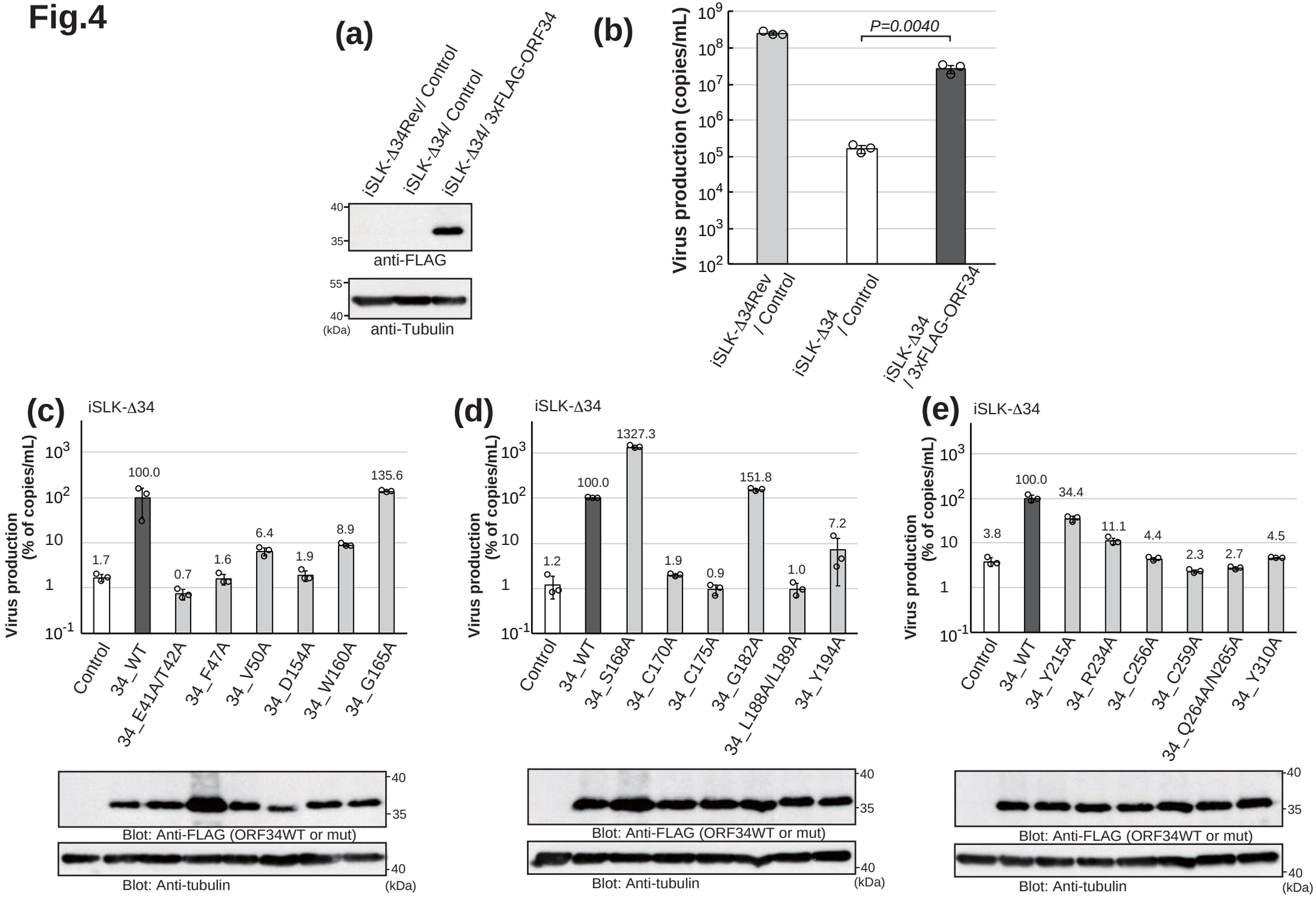
(a)
iSLK-Δ34Rev/ Control
iSLK-Δ34/ Control
iSLK-Δ34/ 3xFLAG-ORF34
40
35
anti-FLAG
55
40
(kDa)
anti-Tubulin
(b)
Virus production (copies/mL)
P=0.0040
iSLK-Δ34Rev / Control
iSLK-Δ34 / Control
iSLK-Δ34 / 3xFLAG-ORF34
(c)
iSLK-Δ34
Virus production (% of copies/mL)
1.7
100.0
0.7
1.6
6.4
1.9
8.9
135.6
Control
34_WT
34_E41A/T42A
34_F47A
34_V50A
34_D154A
34_W160A
34_G165A
Blot: Anti-FLAG (ORF34WT or mut)
Blot: Anti-tubulin
(kDa)
(d)
iSLK-Δ34
Virus production (% of copies/mL)
1.2
100.0
1327.3
1.9
0.9
151.8
1.0
7.2
Control
34_WT
34_S168A
34_C170A
34_C175A
34_G182A
34_L188A/L189A
34_Y194A
Blot: Anti-FLAG (ORF34WT or mut)
Blot: Anti-tubulin
(kDa)
(e)
iSLK-Δ34
Virus production (% of copies/mL)
3.8
100.0
34.4
11.1
4.4
2.3
2.7
4.5
Control
34_WT
34_Y215A
34_R234A
34_C256A
34_C259A
34_Q264A/N265A
34_Y310A
Blot: Anti-FLAG (ORF34WT or mut)
Blot: Anti-tubulin
(kDa)

Fig.5

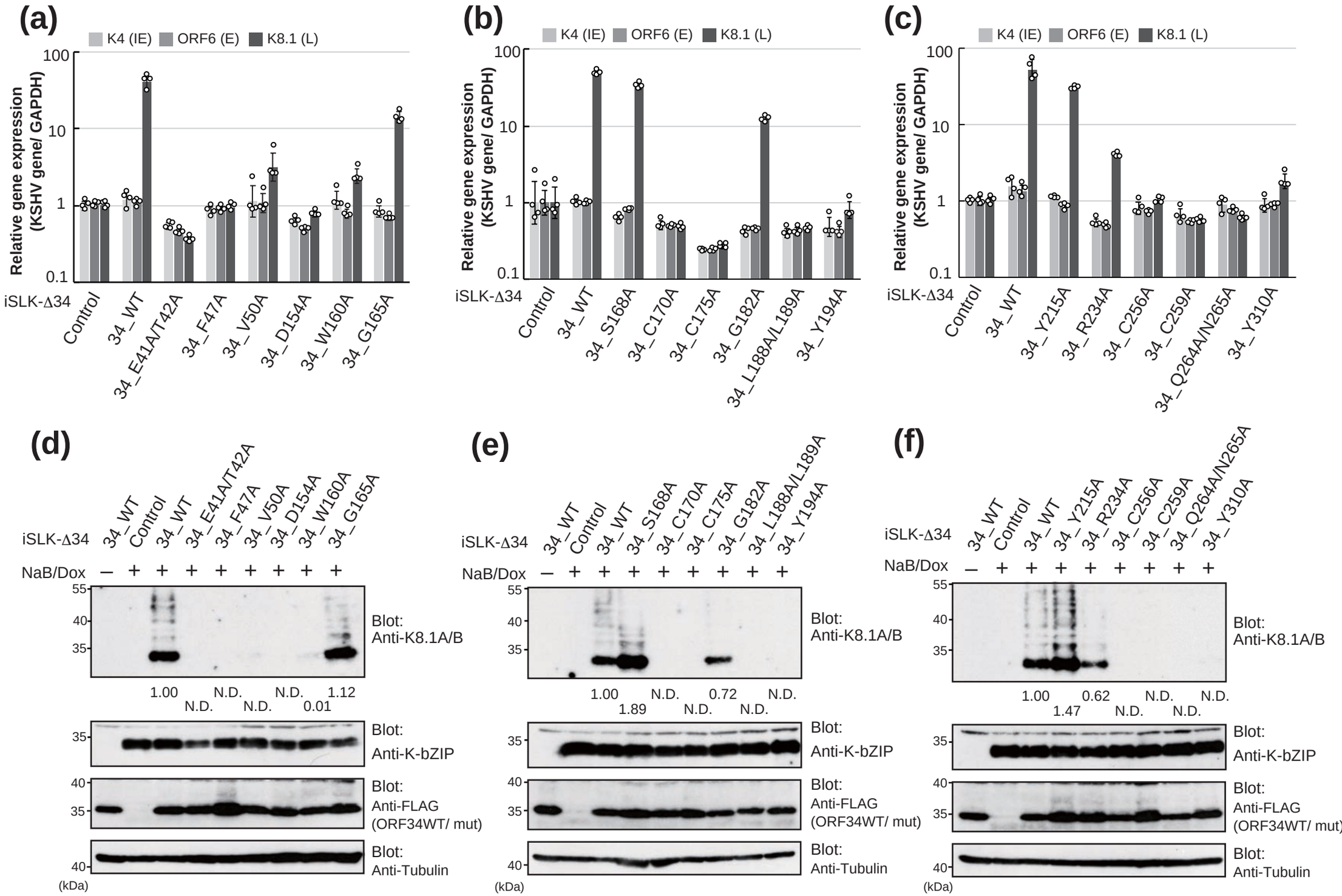
(a)
K4 (IE)
ORF6 (E)
K8.1 (L)
Relative gene expression (KSHV gene/ GAPDH)
100
10
1
0.1
iSLK-Δ34
Control
34_WT
34_E41A/T42A
34_F47A
34_V50A
34_D154A
34_W160A
34_G165A
(b)
K4 (IE)
ORF6 (E)
K8.1 (L)
Relative gene expression (KSHV gene/ GAPDH)
iSLK-Δ34
Control
34_WT
34_S168A
34_C170A
34_C175A
34_G182A
34_L188A/L189A
34_Y194A
(c)
K4 (IE)
ORF6 (E)
K8.1 (L)
Relative gene expression (KSHV gene/ GAPDH)
iSLK-Δ34
Control
34_WT
34_Y215A
34_R234A
34_C256A
34_C259A
34_Q264A/N265A
34_Y310A
(d)
iSLK-Δ34
34_WT
Control
34_WT
34_E41A/T42A
34_F47A
34_V50A
34_D154A
34_W160A
34_G165A
NaB/Dox
– + + + + + + + +
55
40
35
Blot: Anti-K8.1A/B
1.00 N.D. N.D. 1.12
N.D. N.D. 0.01
35
Blot: Anti-K-bZIP
40
35
Blot: Anti-FLAG (ORF34WT/ mut)
40
Blot: Anti-Tubulin
(kDa)
(e)
iSLK-Δ34
34_WT
Control
34_WT
34_S168A
34_C170A
34_C175A
34_G182A
34_L188A/L189A
34_Y194A
NaB/Dox
– + + + + + + + +
55
40
35
Blot: Anti-K8.1A/B
1.00 N.D. 0.72 N.D.
1.89 N.D. N.D.
35
Blot: Anti-K-bZIP
40
35
Blot: Anti-FLAG (ORF34WT/ mut)
40
Blot: Anti-Tubulin
(kDa)
(f)
iSLK-Δ34
34_WT
Control
34_WT
34_Y215A
34_R234A
34_C256A
34_C259A
34_Q264A/N265A
34_Y310A
NaB/Dox
– + + + + + + + +
55
40
35
Blot: Anti-K8.1A/B
1.00 0.62 N.D. N.D.
1.47 N.D. N.D.
35
Blot: Anti-K-bZIP
40
35
Blot: Anti-FLAG (ORF34WT/ mut)
40
Blot: Anti-Tubulin
(kDa)

Fig.6

	ORF34 WT/mutant	ORF66 binding	ORF24BD binding	K8.1 mRNA expression	K8.1 protein expression	Virus production
	S168A	0.969	0.940	0.680	1.889	13.272
Group 1	**WT**	1.000	1.000	1.000	1.000	1.000
Group 1	G165A	0.022	0.680	0.343	1.128	1.356
Group 1	G182A	0.359	1.286	0.250	0.725	1.518
Group 2	C256A	N.D.	0.109	0.020	N.D.	0.044
Group 2	C259A	N.D.	0.027	0.011	N.D.	0.023
Group 2	C170A	0.057	0.325	0.010	N.D.	0.019
Group 2	C175A	0.039	0.345	0.006	N.D.	0.009
Group 2	W160A	0.289	0.473	0.059	0.013	0.089
Group 2	D154A	0.284	0.512	0.019	N.D.	0.019
Group 2	L188A/L189A	N.D.	0.503	0.009	N.D.	0.010
Group 3	R234A	0.775	0.740	0.077	0.626	0.111
Group 3	V50A	1.114	0.861	0.078	N.D.	0.064
Group 3	E41A/T42A	1.033	0.877	0.009	N.D.	0.007
Group 3	F47A	1.086	0.859	0.023	N.D.	0.016
Group 4	Y215A	0.167	1.023	0.572	1.477	0.344
Group 4	Y310A	0.173	0.956	0.036	N.D.	0.045
Group 4	Y194A	0.003	0.645	0.017	N.D.	0.072
Group 4	Q264A/N265A	N.D.	0.666	0.012	N.D.	0.027

Fig.7

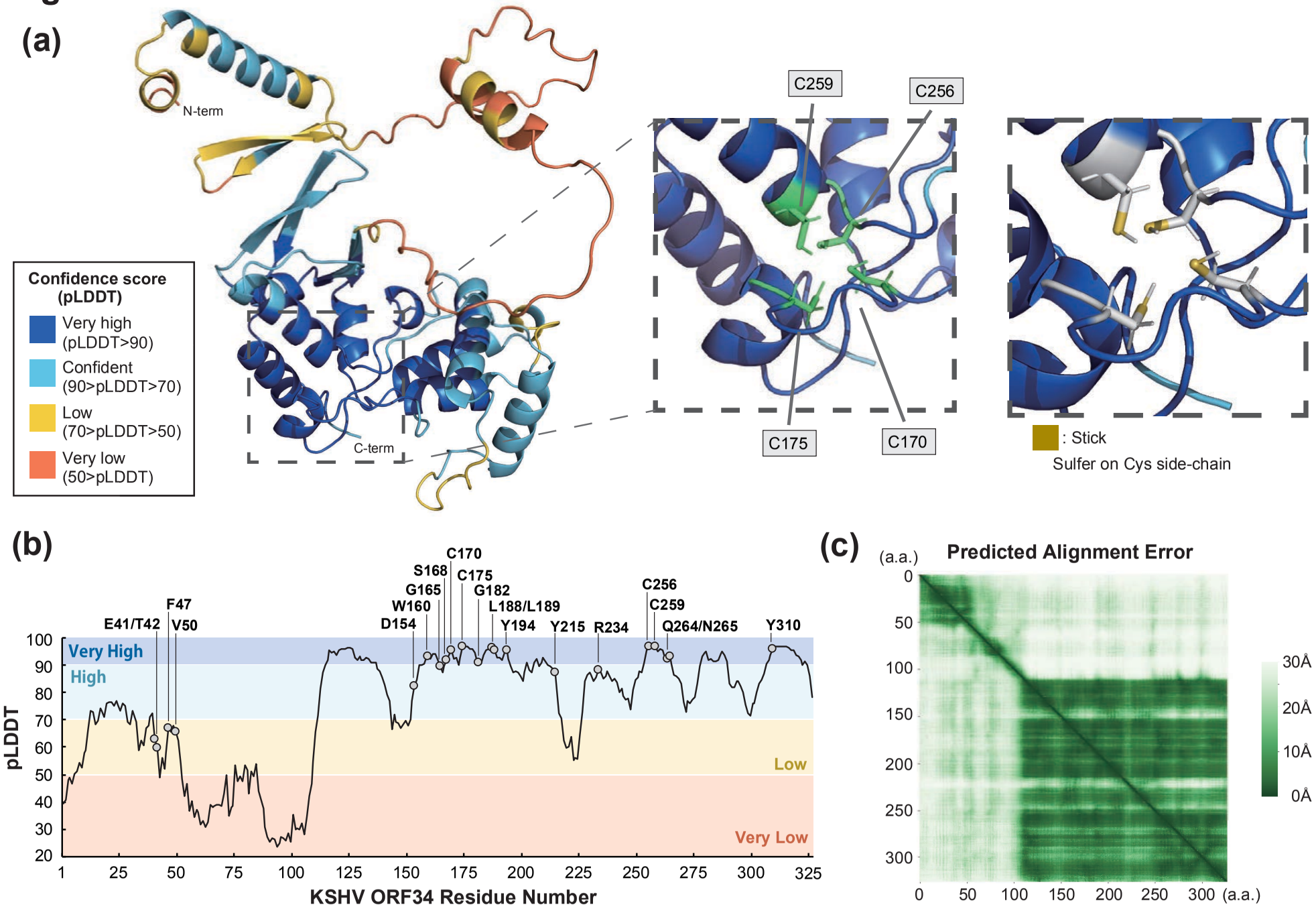
(a)
N-term
C-term
Confidence score (pLDDT)
Very high (pLDDT>90)
Confident (90>pLDDT>70)
Low (70>pLDDT>50)
Very low (50>pLDDT)
C259
C256
C175
C170
: Stick
Sulfer on Cys side-chain
(b)
E41/T42
F47
V50
D154
W160
G165
S168
C170
C175
G182
L188/L189
Y194
Y215
R234
C256
C259
Q264/N265
Y310
Very High
High
Low
Very Low
pLDDT
KSHV ORF34 Residue Number
(c)
Predicted Alignment Error
(a.a.)
30Å
20Å
10Å
0Å

Fig. 8

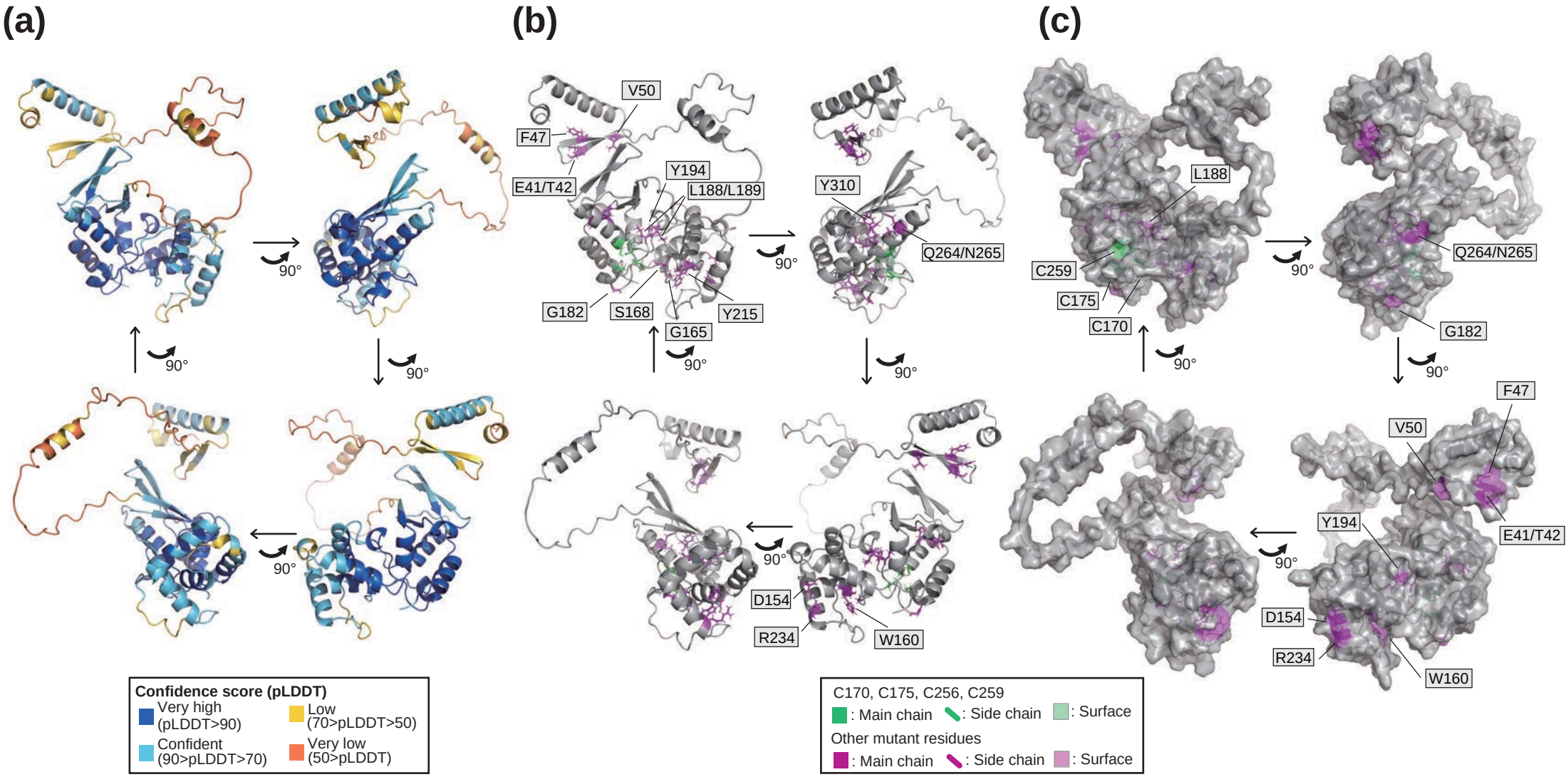
(a)
(b)
(c)
90°
V50
F47
E41/T42
Y194
L188/L189
G182
S168
G165
Y215
Y310
Q264/N265
D154
R234
W160
L188
C259
C175
C170
Confidence score (pLDDT)
Very high (pLDDT>90)
Low (70>pLDDT>50)
Confident (90>pLDDT>70)
Very low (50>pLDDT)
C170, C175, C256, C259
: Main chain
: Side chain
: Surface
Other mutant residues
: Main chain
: Side chain
: Surface

Fig.9

(a)

Binding ion	Binding residues	Template	Score
Cu^{+}	256C, 259C	5vdf_A0	6.519
Zn^{2+}	170C, 175C, 256C, 259C	5xfp_B0	5.468
Fe^{3+}	170C, 175C, 256C, 259C	3lmc_A0	5.272
Fe^{2+}	170C, 175C, 256C, 259C	5v27_A1	3.996
Pb^{2+}	175C, 255T, 256C, 259C	1iw7_D1	3.779
Cd^{2+}	256C, 259C	1fe0_A0	3.658
Cd^{2+}	255T, 256C, 259C	3cjk_B0	3.655
Zn^{2+}	170C, 177Y, 256C, 259C	4c4a_A0	3.394
Zn^{2+}	170C, 175C, 256C	5obz_B0	3.325
Hg^{2+}	170C, 175C, 176L, 256C	1r0g_A0	3.299
Fe^{2+}	170C, 175C, 177Y, 256C	5v27_A1	3.171
Zn^{2+}	256C, 259C	4a46_C0	3.087
Hg^{2+}	256C, 259C	1l8d_A0	3.082
Zn^{2+}	170C, 175C, 177Y, 256C	4mvt_B0	3.053

(b)

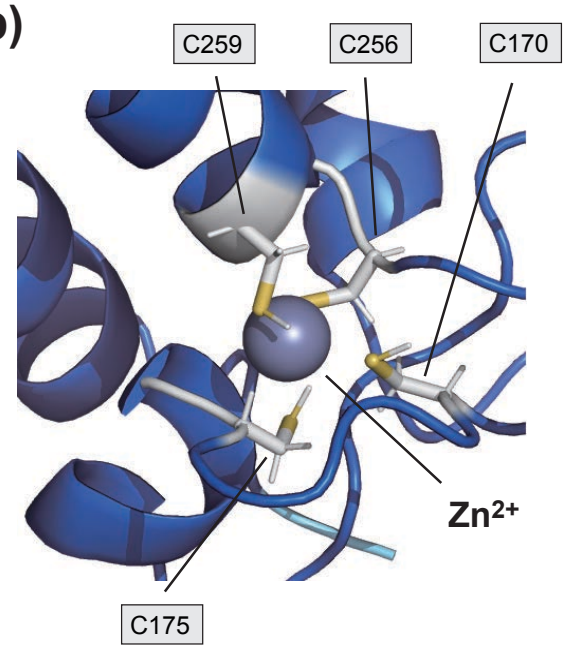

(c)

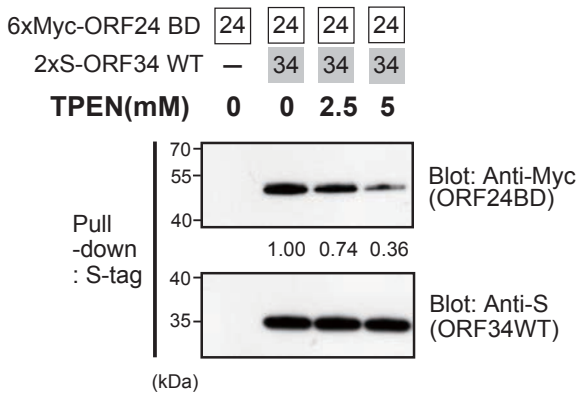

(d)

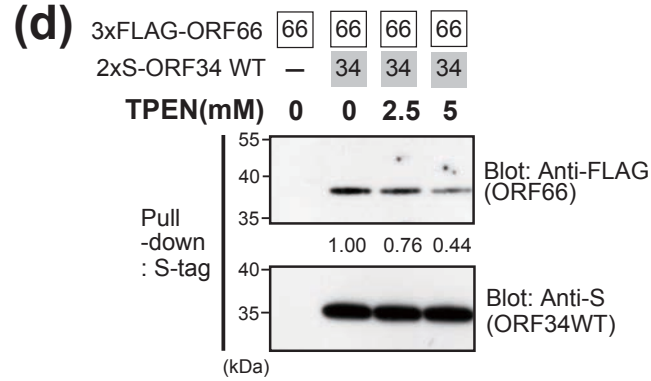

Table 1: Primers for Construction of expression plasmids and RT-qPCR

Primer name	Primer sequences (5' -> 3')
[Cloning expression plasmid]	**a*
S-EcoRI-kshvORF34	acatgaattcATGTTTGCTTTGAGCTCGC
As-kshvORF34-SalI	ctaagtcgacTTAGAGTTGGTTGAGTCCATTCTCC
S_MluI-ORF24BD(1-400)	catacgcgtATGGCAGCGCTCGAGGGC
As_ORF24BD(1-400)-XbaI	taatctagaTTAGCCCAGAGTCCGCGCGTCCGTG
- ORF34 Alanin-scanning mutants	**b*
S_ORF34_Asc1_E41AT42A	tgata**GCAGCT**cccctgaacag
As_ORF34_Asc1_E41AT42A	gggg**AGCTGC**tatcaacttaaattgtc
S_ORF34_Asc2_F47A	aacagc**GCC**ctcttggtttcc
As_ORF34_Asc2_F47A	caagag**GGC**gctgttcaggg
S_ORF34_Asc3_V50A	ctcttg**GCA**tccaacgtgatgc
As_ORF34_Asc3_V50A	ttgga**TGC**caagaggaagctg
S_ORF34_Asc4_D154A	ctgac**GCC**ccccttccgttg
As_ORF34_Asc4_D154A	ggg**GGC**gtcaggaagaagac
S_ORF34_Asc5_W160A	gttgcta**GCG**ctgctgttcaac
As_ORF34_Asc5_W160A	agcag**CGC**tagcaacggaag
S_ORF34_Asc6_G165A	tgttcaac**GCT**cccgcctc
As_ORF34_Asc6_G165A	gcggg**AGC**gttgaacagcag
S_ORF34_Asc7_S168A	acccgcc**GCG**ttttgtcg
As_ORF34_Asc7_S168A	acaaaa**CGC**ggcgggtcc
S_ORF34_Asc8_C170A	ctttt**GCT**cgggccgactgttg
As_ORF34_Asc8_C170A	gcccg**AGC**aaaagaggcgg
S_ORF34_Asc9_C175A	gactgt**GCC**ctgtacaagcagc
As_ORF34_Asc9_C175A	gtacag**GGC**acagtcggccc
S_ORF34_Asc10_G182A	gcagcactgc**GCA**tacccg
As_ORF34_Asc10_G182A	cgggta**TGC**gcagtgctgc
S_ORF34_Asc11_L188AL189A	gtg**GCAGCT**ccaggtcacatg
As_ORF34_Asc11_L188AL189A	g**AGCTGC**caccgggccc
S_ORF34_Asc12_Y194A	catg**GCC**gctcccaaacgg
As_ORF34_Asc12_Y194A	ggagc**GGC**catgtgacctgg
S_ORF34_Asc13_Y215A	gtttcta**GCC**ggagatttttccggg
As_ORF34_Asc13_Y215A	ctcc**GGC**tagaaacttggtgtacttc
S_ORF34_Asc14_R234A	gctacttct**GCC**atacaaagggtagtgag
As_ORF34_Asc14_R234A	ctttgtat**GGC**agaagtagcgaatggc
S_ORF34_Asc15_C256A	acacc**GCC**ctcttgTGTcacatatatc
As_ORF34_Asc15_C256A	agag**GGC**ggtgtgggaaatg
S_ORF34_Asc16_C259A	cctgcctcttg**GCT**cacatatatcag
As_ORF34_Asc16_C259A	tgtg**AGC**caagaggcaggtgtg
S_ORF34_Asc17_Q264AN265A	tcag**GCAGCT**agcataattgcggg
As_ORF34_Asc17_Q264AN265A	atgct**AGCTGC**ctgatatatgtgacac
S_ORF34_Asc18_Y310A	catcg**GCT**gacataccggcgatc
As_ORF34_Asc18_Y310A	atgtc**AGC**cgatgggatgattagatag
[RT-qPCR]	
qPCR_K4-F	TTGTCCGGTCTATGCCAGG
qPCR_K4-R	CTGCCTTGCTTTGTTTGCAA
qPCR_ORF6-F	CTGCCATAGGAGGGATGTTTG
qPCR_ORF6-R	CCATGAGCATTGCTCTGGCT
qPCR_K8.1-F	ACAGATTCGCACAGAAATCCCT
qPCR_K8.1-R	CGAACGATACGTGGGACAATTG
qPCR_GAPDH-F	TCGCTCTCTGCTCCTCCTGTTC
qPCR_GAPDH-R	CGCCCAATACGACCAAATCC

**a* : Underlined lowercase indicates a restriction enzyme site, while uppercase indicates a protein-coding sequence

**b* : Underlined uppercase indicates a mutagenesis site.